

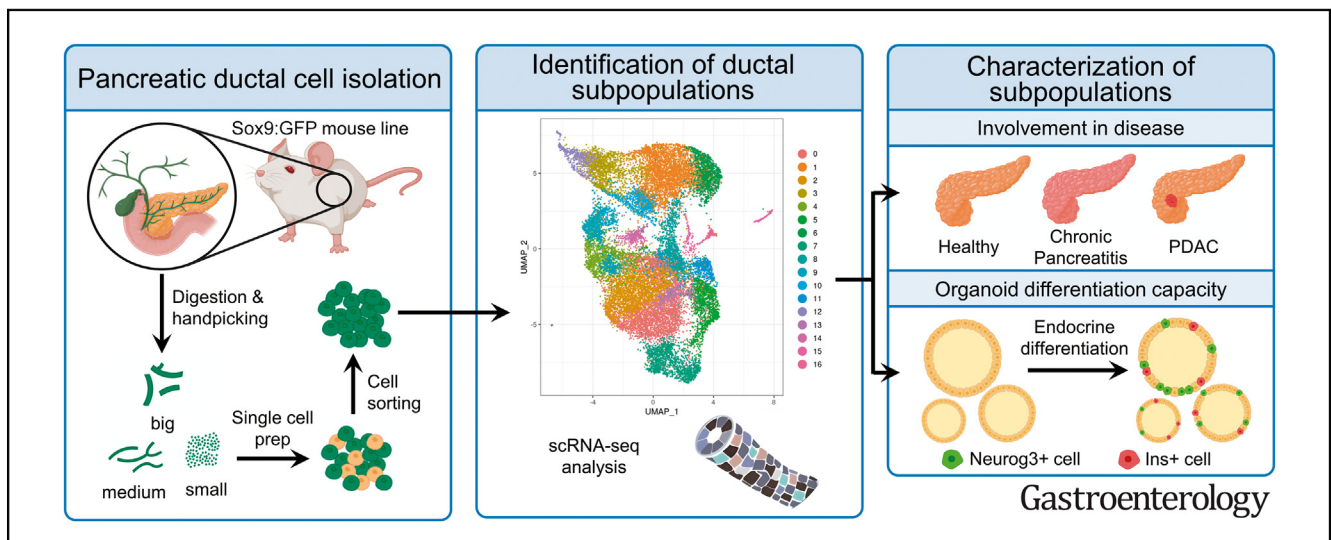
PANCREAS

A Single-Cell Atlas of the Murine Pancreatic Ductal Tree Identifies Novel Cell Populations With Potential Implications in Pancreas Regeneration and Exocrine Pathogenesis



Ángel Fernández,^{1,2,3,4,*} Joan Casamitjana,^{1,2,3,*} Adrián Holguín-Horcajo,^{1,2,3} Katarina Coolens,⁵ Loris Mularoni,³ Li Guo,⁶ Olga Hartwig,⁷ Tim Düking,⁷ Noemi Vidal,⁸ Lincoln N. Strickland,⁹ Lorenzo Pasquali,⁴ Jennifer M. Bailey-Lundberg,⁹ Ilse Roman,⁵ Yue J. Wang,⁶ and Meritxell Rovira^{1,2,3,10}

¹Department of Physiological Science, School of Medicine, Universitat de Barcelona, L'Hospitalet de Llobregat, Spain; ²Pancreas Regeneration: Pancreatic Progenitors and Their Niche Group, Regenerative Medicine Program, Instituto de Investigación Biomédica de Bellvitge - IDIBELL, L'Hospitalet de Llobregat, Spain; ³Program for Advancing the Clinical Translation of Regenerative Medicine of Catalonia, P-CMR[C], L'Hospitalet de Llobregat, Spain; ⁴Department of Medicine and Life Sciences, Universitat Pompeu Fabra, Barcelona, Spain; ⁵Vrije Universiteit Brussel, Translational Oncology Research Center, Laboratory for Medical and Molecular Oncology, Brussels, Belgium; ⁶Department of Biomedical Sciences, College of Medicine, Florida State University, Tallahassee, Florida; ⁷Miltenyi Biotec B.V. & Co KG, Bergisch Gladbach, Germany; ⁸Pathology Department, Hospital Universitari de Bellvitge, L'Hospitalet de Llobregat, Barcelona, Spain; ⁹Department of Anesthesiology, Critical Care and Pain Medicine, McGovern Medical School, The University of Texas Health Science Center at Houston, Houston, Texas; and ¹⁰CIBER de Diabetes y Enfermedades Metabólicas Asociadas (CIBERDEM), Instituto de Salud Carlos III, Barcelona, Spain



See editorial on page 845.

BACKGROUND & AIMS: Pancreatic ducts form an intricate network of tubules that secrete bicarbonate and drive acinar secretions into the duodenum. This network is formed by centroacinar cells, terminal, intercalated, intracalated ducts, and the main pancreatic duct. Ductal heterogeneity at the single-cell level has been poorly characterized; therefore, our understanding of the role of ductal cells in pancreas regeneration and exocrine pathogenesis has been hampered by the limited knowledge and unexplained diversity within the ductal network. **METHODS:** We used single cell RNA sequencing to comprehensively characterize mouse ductal heterogeneity at single-cell resolution of the entire ductal epithelium from centroacinar cells to the main duct. Moreover, we used organoid cultures, injury models, and pancreatic tumor samples to interrogate the role of novel ductal

populations in pancreas regeneration and exocrine pathogenesis. **RESULTS:** We have identified the coexistence of 15 ductal populations within the healthy pancreas and characterized their organoid formation capacity and endocrine differentiation potential. Cluster isolation and subsequent culturing let us identify ductal cell populations with high organoid formation capacity and endocrine and exocrine differentiation potential in vitro, including a Wnt-responsive population, a ciliated population, and Flrt3⁺ cells. Moreover, we have characterized the location of these novel ductal populations in healthy pancreas, chronic pancreatitis, and tumor samples. The expression of Wnt-responsive, interferon-responsive, and epithelial-to-mesenchymal transition population markers increases in chronic pancreatitis and tumor samples. **CONCLUSIONS:** In light of our discovery of previously unidentified ductal populations, we unmask potential roles of specific ductal populations in pancreas regeneration and exocrine pathogenesis. Thus, novel lineage-tracing

models are needed to investigate ductal-specific populations in vivo.

Keywords: Ductal Cells; scRNA-Seq; Organoids; Exocrine Pathologies; Pancreas Regeneration.

Pancreatic ducts form an intricate network of tubules. The first cells of the ductal epithelium touching the acini are centroacinar cells (CACs), located at the tip of terminal/intercalated ducts that will later join to form larger intralobular ducts that fuse into interlobular ducts to empty acinar secretions into the main duct. The main duct merges with the common bile duct and opens into the duodenum through the duct of Wirsung.¹ Ductal cells secrete an alkaline mucus fluid rich in bicarbonate to neutralize the stomach's acidic chyme. Moreover, ductal cells play a key role in the development of pancreatic exocrine pathologies, such as cystic fibrosis, pancreatitis, and pancreatic ductal adenocarcinoma (PDAC).¹ Notably, well-differentiated PDAC carries the morphologic appearance of ductal structures expressing ductal markers.² Thus, by histology alone, the putative cell of origin was long thought to be ductal.³ However, recent studies demonstrated that both acinar and ductal cells can be transformed upon *KRAS* mutations.⁴

Tissue-resident progenitors have been studied in highly proliferative and regenerative tissues, like the intestine,⁵ where progenitors comprise 5%–8% of the tissue.⁶ However, the pancreas has low proliferation rates and limited regeneration capacity; thus, the progenitor reservoir, if any, is likely modest. Ductal cells, in the mammalian pancreas, have attracted most of the attention as potential sources of new β cells for several reasons: (1) Several studies observed endocrine cells near to or embedded in the ducts during growth or regeneration.^{7,8} (2) Ductal and endocrine cells share a common progenitor during development. Neurogenin3⁺ cells within these progenitors delaminate and differentiate into endocrine cells, while the remaining duct-like complexes differentiate into mature ducts.⁹ (3) Moreover, lineage tracing of ductal cells in zebrafish demonstrated that they are progenitors in adult tissue.¹⁰ Therefore, it stands to reason that ductal cells may play a role in pancreas regeneration. However, this is a highly controversial topic because several lineage tracing studies using panductal markers showed no β -cell neogenesis from ducts (reviewed by Afelik and Rovira¹¹ and Magenheimer et al¹²). (4) Finally, ductal cells acquire cellular plasticity in vitro because they can uniquely form organoids,¹³ an ability solely displayed by adult progenitors.¹⁴

Although the ductal network is a complex system, it is mostly seen as a homogeneous population, and little is known about ductal heterogeneity in mammals and the implications of different ductal populations in exocrine pathogenesis and regeneration. Single-cell technologies now allow the investigation of the transcriptome of individual cells, dissecting tissue, and cell heterogeneity beyond what was possible with bulk approaches. Importantly, ductal pancreatic cells have been vastly underrepresented in single-cell analysis for several reasons: (1) Most studies

WHAT YOU NEED TO KNOW

BACKGROUND AND CONTEXT

A comprehensive characterization of mouse ductal heterogeneity has been poorly characterized due to technical limitations and isolation techniques.

NEW FINDINGS

We have characterized the entire ductal epithelium of the mouse pancreas at single-cell resolution, identifying an unforeseen level of heterogeneity, highlighting the coexistence of 15 ductal populations, and investigated their role in exocrine pathogenesis and pancreas regeneration.

LIMITATIONS

Our results in organoid cultures, exocrine injury models, and pancreatic cancer samples highlight the potential role of novel ductal populations in regeneration and exocrine pathogenesis. Still, novel animal models are needed to further investigate our results in vivo.

CLINICAL RESEARCH RELEVANCE

The translation of our findings into human settings could identify different ductal cells of origin of pancreatic cancer and lead to novel stratification of PDAC patients according to ductal markers that may affect prediction outcomes and identify novel therapeutic targets. Moreover, our results in endocrine differentiation in organoid cultures could result in future cell replacement therapies for diabetes treatment.

BASIC RESEARCH RELEVANCE

Our data lay the foundation for future studies to investigate the role of novel ductal populations in pancreas regeneration and exocrine pathogenesis in novel mouse models in vivo.

have centered their interest in isolated islets, containing few ducts.¹⁵ (2) Digestive enzymes cause degradation of cells and RNA. (3) Ducts represent ~10%¹ of the gland but are refractory to disaggregation; thus, low heterogeneity has been described.^{16,17} (4) Single nuclei RNA sequencing of frozen human pancreas has circumvented digestive enzyme activity,¹⁸ but, again, ducts are underrepresented.

Here, we investigated ductal heterogeneity of the entire ductal network using a mouse transgenic line where GFP

* Authors share co-first authorship.

Abbreviations used in this paper: ADM, acinar-to-ductal metaplasia; CAC, centroacinar cell; CP, chronic pancreatitis; EMT, epithelial-to-mesenchymal transition; FACS, fluorescence-activated cell sorting; HPC, *LSL-Kras^{G12V};Trp53^{R172H/+};Hnf1bCreERT2*; IAD, intralobular duct; IED, intercalated duct; IFN, interferon; KPC, *LSL-Kras^{G12D/+};LSL-Trp53^{R172H/+};Pdx-1-Cre*; mRNA, messenger RNA; ns, not significant; PanIN, pancreatic intraepithelial neoplasia; PDAC, pancreatic ductal adenocarcinoma; PDG, pancreatic ductal gland; qPCR, quantitative polymerase chain reaction; scRNA, single cell RNA sequencing; SSC, side scatter; T1D, type 1 diabetes; TD, terminal duct; UMAP, Uniform Manifold Approximation and Projection.

 Most current article

© 2024 The Author(s). Published by Elsevier Inc. on behalf of the AGA Institute. This is an open access article under the CC BY-NC-ND license (<http://creativecommons.org/licenses/by-nc-nd/4.0/>).

0016-5085

<https://doi.org/10.1053/j.gastro.2024.06.008>

expression is driven by *Sox9* promoter, labeling all ductal cells.¹⁹ We observed increased organoid formation capacity in medium-big duct-derived organoids with lower *Sox9* expression compared to small ducts. Moreover, the capacity to give rise to endocrine progenitors as well as insulin-producing and somatostatin-producing cells was significantly higher in medium-big duct-derived organoids. Furthermore, we have comprehensively characterized mouse ductal heterogeneity at single-cell resolution, highlighting the coexistence of 15 ductal clusters. Importantly, we have also identified surface markers, allowing the isolation of several novel ductal populations, and assessed their plasticity in functional studies in organoid cultures, showing that ductal populations located in medium-big size ducts have a higher progenitor capacity defined by organoid formation efficiency and increased endocrine/exocrine differentiation potential. Finally, we have characterized tissue expression and localization of these previously unidentified ductal populations in mouse adult pancreas, chronic pancreatitis (CP), and mouse and human PDAC. Our results suggest that populations located in medium-big ducts could play a key role in exocrine pathogenesis and tumorigenesis.

Materials and Methods

Mice

Tg(Sox9-EGFP)EB209Gsat was obtained from the J. Ferrer laboratory. Experimental procedures on 8–16-week-old mice were approved by the Animal Experimentation Ethics Committee at the Instituto de Investigación Biomédica de Bellvitge (IDIBELL) (approval no. AR18009). Mice were housed at the IDIBELL animal facility under specific pathogen-free conditions in accordance with the institutional guidelines and ethical regulations. Genotyping primers are provided in [Supplementary Table 1](#).

Chronic Pancreatitis

CP mice were housed under standardized specific pathogen-free conditions, and experiments were approved by the Ethical Committee for Animal Experiments of the Vrije Universiteit Brussel and carried out according to the national guidelines on animal experimentation. For CP induction, 8–12-week-old C57BL/6 mice were treated with 125 $\mu\text{g}/\text{kg}$ caerulein.²⁰ Further details are provided in the [Supplementary Methods](#).

Pancreatic Ductal Adenocarcinoma Models

Two mouse models of PDAC have been used in our studies. First, *Pdx-1-Cre* mice were crossed with *LSL-Trp53^{R172H/+}* and *LSL-Kras^{G12D/+}* mice to obtain *LSL-Kras^{G12D/+};LSL-Trp53^{R172H/+};Pdx-1-Cre* (KPC), in accordance with institutional ethical guidelines and approved by St. Vincent's Hospital Animal Ethics Committee, Sydney, Australia (approval no. 16/02). The second mouse model was used to trace ductal-derived tumors as previously published,²¹ *LSL-Kras^{G12V};Trp53^{R172H/+};Hnf1bCreERT2* (HPC).

Human Pancreatic Ductal Adenocarcinoma Samples

Human PDAC samples were collected from the Bellvitge Hospital Biobank HUB-ICO-IDIBELL. The study included

formalin-fixed, paraffin-embedded pancreatic cancer tissue blocks selected from the Anatomopathology Department of Bellvitge Hospital. Ethical consent was given by the Research Ethics Committee at the Bellvitge Hospital (BB23-50).

Duct Isolation

Mouse pancreas digestion followed previously published protocols²² with minor modifications. Whole ducts were hand-picked and sorted by size under a fluorescent stereoscope. Further details are provided in the [Supplementary Methods](#).

Single-Cell Prep

Small, medium, and big ducts were digested with tryPLE Express (Gibco) for 5 to 10 minutes at 37°C, with the digestion mix vigorously shaken every 2–3 minutes. Purified single ductal cells were resuspended in fluorescence-activated cell sorting (FACS) buffer. Further details are provided in the [Supplementary Methods](#).

Fluorescence-Activated Cell Sorting Analysis

For FACS analysis, antibody incubation was performed following the manufacturer's instructions ([Supplementary Table 2](#) and [Supplementary Methods](#)). FACS was performed using a Beckman Coulter High-Speed Cell Sorter Moflo-XDP. Flow-derived data were analyzed using Kaluza 2.1 (Beckman Coulter, Inc).

Organoid Culture

Whole ducts or FACS-sorted ductal cells (GFP⁺) were embedded in Matrigel (Corning) at a density of 1000–5000 cells in 24-well plates and cultured in pancreatic organoid expansion media ([Supplementary Table 2](#) and [Supplementary Methods](#)).

Endocrine Differentiation

Two days after organoid passage, organoid differentiation was induced with endocrine differentiation medium ([Supplementary Table 2](#) and [Supplementary Methods](#)).

Immunostainings

Staining details are included in the [Supplementary Methods](#). Antibodies are shown in [Supplementary Table 2](#). Confocal images were captured by a Leica TCS_SP5 Confocal. Epifluorescent images were acquired on a Zeiss Axio Observer Z1 Apotome inverted fluorescent microscope. Organoid brightfield images were taken on a Leica Z16 APO stereomicroscope. Organoid sizes were measured using ImageJ/FIJI (National Institutes of Health). Quantification of marker expression was performed using Imaris9.6 (Oxford Instruments). Multiplex immunofluorescence methods using MACSima Imaging Cyclic Staining technology (Miltenyi Biotec) are included in the [Supplementary Methods](#).

RNA Isolation and Quantitative Polymerase Chain Reaction

RNA isolation of primary cells or organoids was performed following the manufacturer's instructions using the RNeasy Mini kit (Qiagen). Extracted RNA was DNase treated and reverse transcribed using the Roche Transcriptor First Strand cDNA Synthesis kit. Quantitative polymerase chain reaction (qPCR) samples were prepared with SYBR Green and marker-

specific primers (Supplementary Table 1). qPCRs were run using the Applied Biosystems 7900HT Real-Time PCR.

Sample Preparation for Single Cell RNA Sequencing

Ten thousand Sox9:eGFP⁺ cells from each ductal fraction were sorted from a pool of 3 male mice (8–12 weeks) in 2 independent experiments. Library preparation of 3' messenger RNA (mRNA) followed 10x Genomics manufacturing instructions. Sequencing was carried out as paired end (PE77) using the NovaSeq6000 (Illumina).

Single Cell RNA Sequencing Analysis

Data quality control, filter, dimension reduction, clustering, and differential expression analysis were performed with the Seurat version 4.1.1 pipeline previously described.²³ Briefly, cells were filtered with nFeature_RNA>200, nFeature_RNA<6000, percent.mt<5, and nCount_RNA<50,000. Sctransform was used to normalize the data and regress out potential sample batch effects. RunPCA, RunUMAP, FindNeighbors, and FindClusters (resolution 0.6) were then sequentially applied to perform dimension reduction and cell clustering. FindAllMarkers was then called with min.pct=0.1 and logfc.threshold=0.25 to identify markers for each clusters.

Statistical Analysis

Unless specified in the figure legends, all *P* values were calculated using GraphPad Prism 10 (GraphPad Software LLC) with the following significance: not significant (ns): *P* > .05; **P* < .05; ***P* < .01; ****P* < .001; *****P* < .0001. Statistical tests used are specified in the figure legends.

Results

Different Organoid Formation Potential of Ductal Compartments Fractionated by Size

Ductal cells can form organoids in culture upon the addition of developmental cues in the medium mimicking the niche,¹³ although it is not known if all pancreatic ductal cells display equal organoid formation capacity. Thus, we investigated if ductal cells from different compartments of the ductal tree, including CACs, terminal ducts (TDs), intracalated ducts (IADs), intercalated ducts (IEDs), and the main duct display different capacities for organoid formation (Figure 1A and B). Upon pancreas digestion, we isolated small (<50 μm, including CACs and TDs), medium (50–200 μm, including small IADs and small IEDs), and big ducts (>200 μm, including big IADs, big IEDs, and the main duct) guided by a Sox9:eGFP transgenic line (Figure 1B and C). This line recapitulates Sox9 expression in all tissues, including the pancreas,¹⁹ where the entire ductal epithelium expresses Sox9⁹ (Figure 1B–D). While all the fractions formed organoids, medium-big ducts form bigger organoids in a short period of time (Figure 1E).

Bigger Ducts Display Higher Organoid Formation Capacity

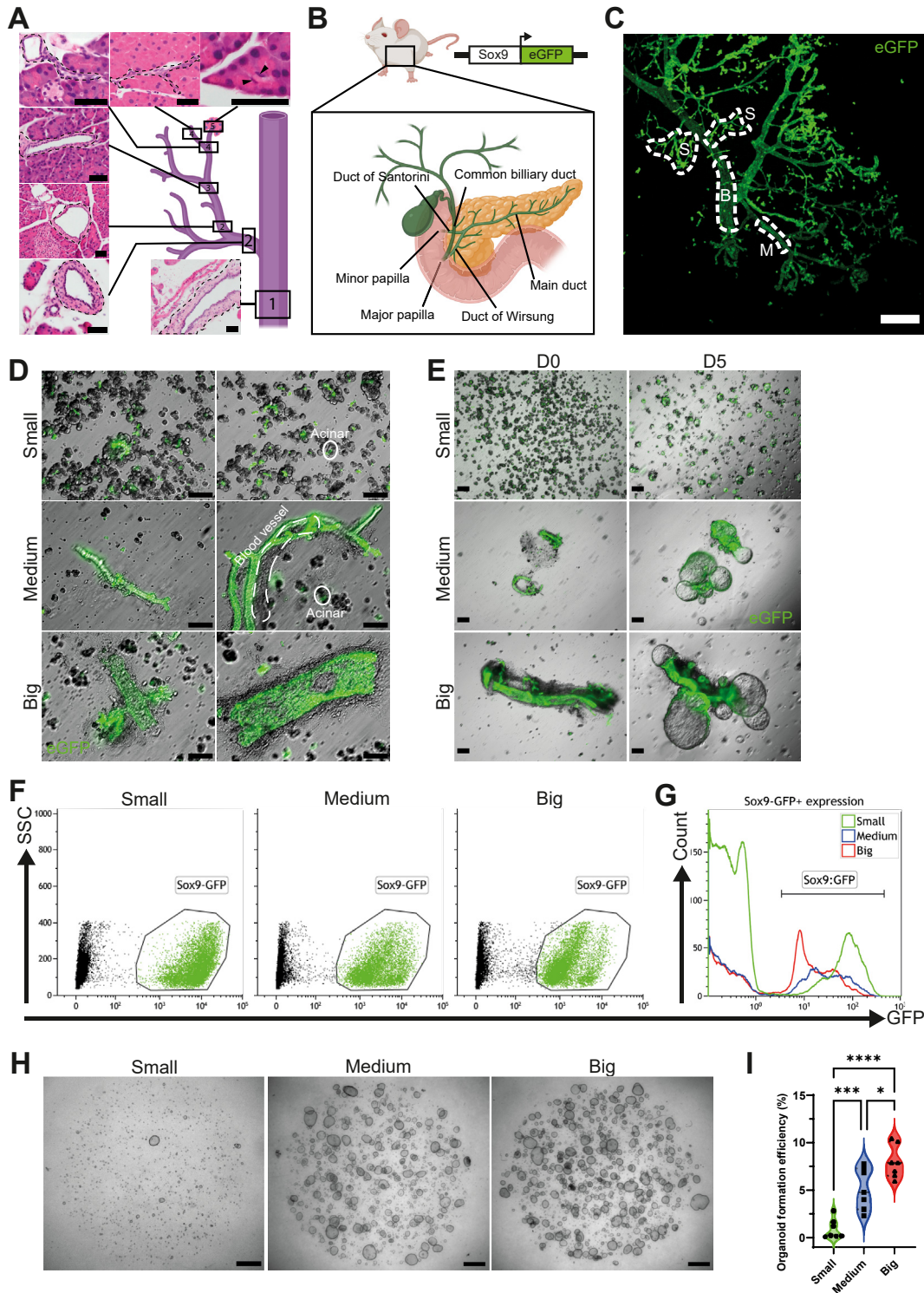
To ensure that the different organoid formation ability is not due to (1) a higher number of cells in bigger ducts; (2)

signaling from vessels, connective tissue, extracellular matrix, or mesenchyme, enriched in big ducts; or (3) a counterproductive effect of acinar cells enriched in small duct fractions (Figure 1D and E), we FACS-isolated Sox9:eGFP⁺ cells from each fraction (Figure 1F). The isolation of ductal cells highlighted Sox9 heterogeneous expression, showing a reduction of Sox9:eGFP intensity as ductal size increases (Figure 1F and G). Isolated ductal cells were plated at the same density to test organoid formation capacities. Big and medium duct-derived organoids showed higher organoid formation efficiency in number and size (Figure 1H and I and Supplementary Figure 1A): 0.89% ± 1.03% for small, 5.11% ± 2.16% for medium, and 7.93% ± 1.73% for big duct-derived organoids.

Medium-Big Duct-Derived Organoids Display Increased Potential for Differentiation Into Endocrine Lineages

Organoids expressed classical ductal markers independent of the duct of origin (Figure 2A). However, we observed significant heterogeneity: whereas *Hnf1β* expression was similar in all organoids, *Sox9* and *Spp1* expression levels were lowest in bigger ducts. Genes most highly expressed in big duct-derived organoids included *Krt19* and *Onecut2* (Figure 2A). Further characterization of ductal markers by immunofluorescence in organoids showed a high degree of heterogeneity (Supplementary Figure 1B and C). These results suggest the concurrence of diverse differentiation states or the coexistence of different ductal populations in the original preparation.

Embryonic bipotent progenitors express many ductal cell markers and progressively lose their progenitor capacity as they mature into ducts.⁹ Thus, we analyzed whether organoids from different ductal compartments were transcriptionally similar to a bipotent progenitor (Supplementary Figure 1D). We observed that organoids derived from bigger ducts were closer to a bipotent progenitor based on reduced expression of *Nr5a2*, *Gata4*, and *Pdx1* while maintaining *Gata6* and *Onecut1* (Figure 2B). We therefore asked if this, coupled with the higher organoid formation capacity of bigger ducts and together with the expression of markers closely related to a bipotent progenitor, could also indicate an increased capacity for endocrine differentiation. Thus, we developed a differentiation protocol that mimics embryonic signaling cues (Supplementary Figure 1E). We observed that medium-big duct-derived organoids display higher capacity for differentiation into endocrine progenitors, showing increased *Neurog3* and *NeuroD1* mRNA levels (Figure 2C and Supplementary Figure 2A) and increased *Neurog3* protein levels (Figure 2D and E). Importantly, organoids derived from bigger ducts also display a higher capacity for differentiation into endocrine lineages, including increased mRNA levels of *Sst* and *Ins* but no *Gcg* or *Ppy* (Figure 2C and Supplementary Figure 2B). Interestingly, Insulin⁺ cells did not coexpress *Neurog3*, suggesting that organoid differentiation mimics in vivo embryonic

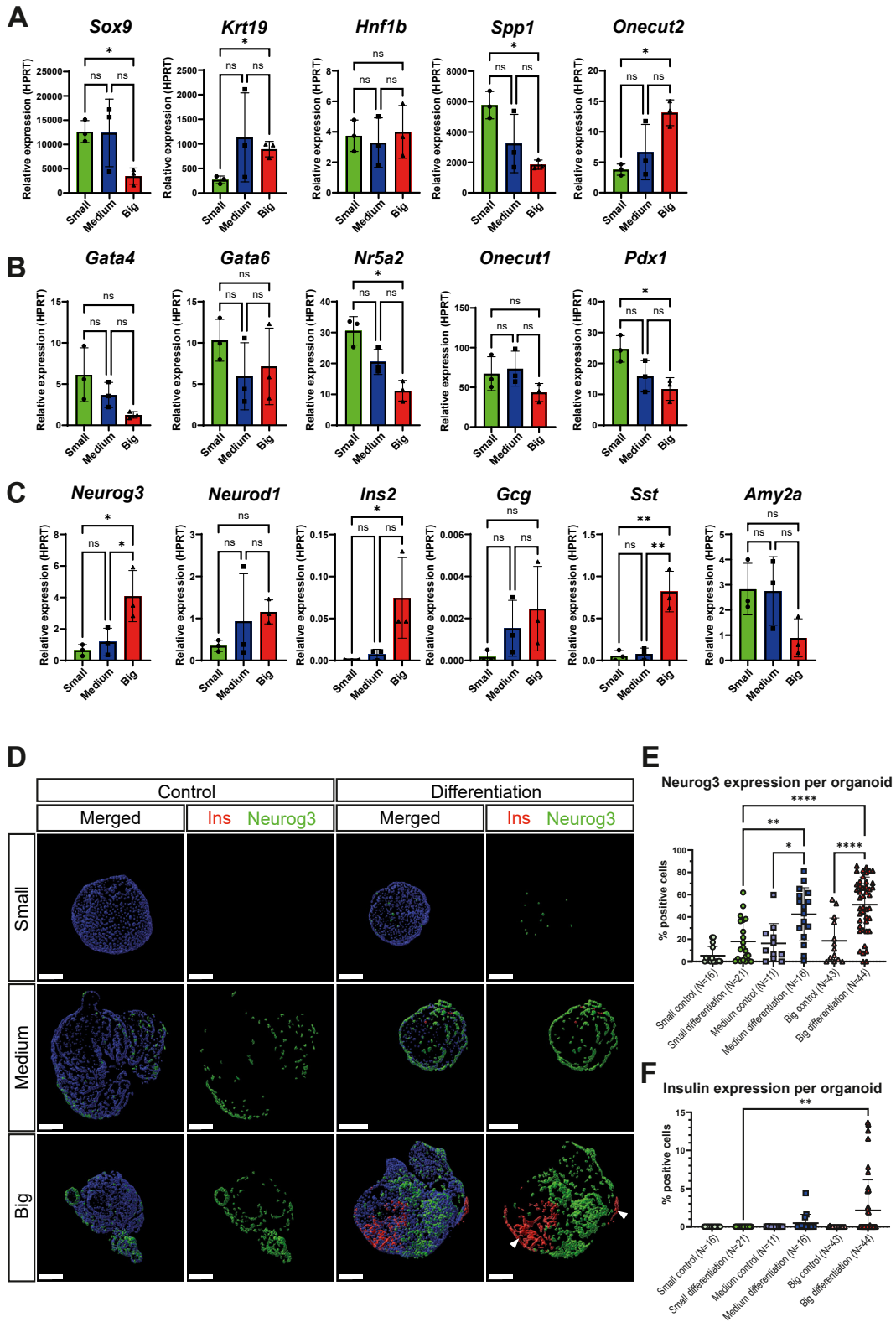


PANCREAS

Figure 1. Organoid formation potential of ductal compartments. (A) Drawing and representative images (H&E) of the pancreatic ductal tree, showing the main duct (1); interlobular (2), intralobular (3), intercalated/terminal (4) ducts; and CACs (5). Dashed lines indicate ducts, and *arrowheads* show CACs. *Scale bars*, 50 μ m. (B) Drawing of the Sox9:eGFP transgenic mouse (created with [BioRender.com](https://www.biorender.com)). (C) Maximum projection of lobular units of Sox9:eGFP pancreas intercalated ducts and CACs (small) and intralobular (medium) and interlobular (big) ducts are highlighted. *Scale bar*, 200 μ m. (D) Representative brightfield images of small, medium, and big ducts hand-picked following digestion. Enriched fractions may have acini, blood vessels, and/or stroma. *Scale bar*, 100 μ m. (E) Ducts cultured at days 0 and 5 in organoid expansion medium. *Scale bars*, 200 μ m. (F) Representative FACS plots of Sox9:eGFP⁺ cells isolated from small, medium, and big ducts. (G) Representative FACS histogram showing Sox9:eGFP levels that increase as the size of the ducts diminishes. (H) Images of organoids plated at the same cell density after 1 week in culture. *Scale bar*, 100 μ m. (I) Violin plot showing organoid formation efficiency (1-way analysis of variance, Tukey post hoc test, N = 7). B, big; M, medium; S, small.

development (Figure 2D-F). Low levels of acinar markers were detected in all organoids (Figure 2C). Finally, the expression of ductal markers was reduced but observed in all organoids (Supplementary Figure 2C). Of note, all

experiments with organoids were made with isolated cells to eliminate duct-resident endocrine cells because the contamination could lead to misinterpretation of the results (Supplementary Figure 2D).



Single Cell RNA Sequencing of Ductal Cells From Mouse Adult Pancreas Identifies Novel Ductal Populations

Encouraged by the observation that ductal compartments behaved differently in organoid cultures, pointing to the existence of different ductal populations, we comprehensively characterized ductal heterogeneity by single cell RNA sequencing (scRNA-seq) of isolated Sox9:eGFP⁺ cells from each ductal compartment, excluding the intrapancreatic bile and common biliary duct and including the main duct (Supplementary Figure 2E), followed by FACS. Because each sample was run independently, we could later identify the origin of each newly identified cluster (Figure 3A–C).

To identify previously unknown ductal populations, we integrated all cells sequenced and filtered out doublets and low-quality cells. Our dataset contained 21,637 cells, and cluster analysis identified 17 populations with an average of 7133 unique molecular identifier/cell and 2706 genes/cell (Figure 3B–D and Supplementary Figure 3A and B). Clustering analysis showed that cells from small ducts cluster separately (Figure 3C). Moreover, we could attribute 5 clusters derived from small duct fractions (clusters 1, 3, 6, 10, and 12), 1 cluster derived from medium ducts (cluster 4), 4 clusters derived from big ducts (clusters 2, 5, 7, and 13), 3 clusters derived from medium-big ducts (clusters 0, 9, and 11), and 4 clusters containing mixed cells (clusters 8 and 14–16) (Supplementary Table 3).

Although all clusters expressed ductal markers (Figure 3E), we observed higher *Krt19* and lower *Sox9* and *Spp1* expression in big duct-derived clusters, especially clusters 7 and 5. *Onecut2* expression was absent in small duct-derived clusters. Finally, *Hnf1β* expression was evenly distributed (Figure 3E and Supplementary Figure 3C). These results correlate with the qPCR analysis in organoids derived from different ductal fractions (Figure 2A).

Identification of Acinar Contaminants but not Endocrine Cells

Further analysis of endocrine lineage-specific markers (*Neurog3*, *Ins*, *Gcg*, *Sst*, and *Ppy*) to investigate the existence of a ductal-endocrine populations showed no expression of endocrine markers (Figure 3F).

On the other hand, the analysis of acinar-specific markers showed high expression in clusters 12 and 3 (Supplementary Figure 4A), suggesting a possible

contamination of acinar cells, ambient RNA, or early acinar-to-ductal metaplasia (ADM). Surprisingly, clusters 12 and 3 also expressed ductal markers (Figure 3E). Thus, to clarify if these clusters represent acinar contaminants or ADM, we sorted side-scatter^{high} (SSC)/Sox9:eGFP⁺/EpCAM⁺ cells (representing GFP⁺ acinar cells) and SSC^{low}/Sox9:eGFP⁺/EpCAM⁺ cells (ductal cells) (Supplementary Figure 4B). Staining for acinar (Amylase) and ductal markers (GFP) of sorted populations clearly showed that SSC^{high}GFP⁺ cells were acinar contaminants because Amylase⁺ cells were GFP⁻ but show a GFP⁺ CAC attached (Supplementary Figure 4C).

Recent single nuclei RNA sequencing studies¹⁸ described 3 acinar populations: idling acinar, secretory acinar, and acinar regenerating. In our scRNA-seq and immunofluorescence, we identified cluster 12 as a secretory acinar population (Amylase^{high}) and cluster 3 as an idling acinar population (Amylase^{low}, idling phenotype) (Supplementary Figure 4D and E).

Novel Ductal Populations

When comparing a cluster to all other clusters, significantly differentially expressed genes highlighted the existence of previously unidentified ductal populations (Figures 3B–D and 4A and Supplementary Table 4).

Clusters derived from small ducts allowed for identifying genes uniquely or highly expressed in CACs/TD. Cluster 6 (*Obp2b* population) is characterized by the expression of *Obp2b*, known to be expressed in the mammary gland²⁴ but not in the pancreas. Cluster 1 (ApoE/C population) expresses apolipoproteins (*ApoC1/ApoE*) associated with PDAC prognosis.²⁵ Cluster 1 is enriched in CACs because it shows the highest levels of *Aldh1b1*, previously described as a CAC marker²⁶ (Supplementary Figure 3E). Cluster 10 (*Wfdc18.2* population) is characterized by high expression of *Wfdc18* related to PDAC.²⁷ Our data indicate that *Prox1* expression is higher in CACs/TDs. *Prox1* plays an important role in pancreas morphogenesis. It is expressed in pancreatic progenitors and gets restricted to islets and some ductal cells in the adult.²⁸ Finally, *Cftr* is highly expressed in small duct-derived/containing clusters. Mutations in *Cftr* produce cystic fibrosis²⁹; therefore, our data suggest that CACs/TD could be the main players in the exocrine damage/blockage observed in cystic fibrosis.

Cluster 4 (*Tesc* population), derived from medium-size ducts, is characterized by the expression of *Tescalcin*,

Figure 2. Organoid differentiation potential into endocrine progenitors and insulin-producing cells. (A) mRNA expression of ductal markers (*Sox9*, *Krt19*, *Hnf1b*, *Spp1*, and *Onecut2*) by qPCR on small, medium, and big duct-derived organoids (Brown-Forsythe and Welch analysis of variance, Dunnett's test 3 post hoc test, N = 3). (B) mRNA expression analysis of genes expressed in multipotent pancreatic and bipotent progenitors (*Gata4*, *Gata6*, *Nr5a2*, *Onecut1*, and *Pdx1*) on organoids (Brown-Forsythe and Welch analysis of variance, Dunnett's T3 post hoc test, N = 3). (C) Endocrine/exocrine differentiation was assessed by qPCR analysis of *Neurog3*, *NeuroD1*, *Ins2*, *Gcg*, *Sst*, and *Amy2a* mRNA levels on duct-derived organoids upon differentiation (1-way analysis of variance, Tukey post hoc test, N = 3). Relative expression instead of fold-change vs control was used when no expression was detected in control samples. (D) Representative immunofluorescence images of differentiated organoids toward the endocrine lineage. Insulin (red, white arrowheads) and Neurog3 (green) expression in control and differentiated organoids. Scale bar, 50 μm. (E, F) Quantification of (E) Neurog3⁺ and (F) Insulin⁺ cells per organoid in control and differentiated organoids (1-way analysis of variance, Tukey post hoc test).

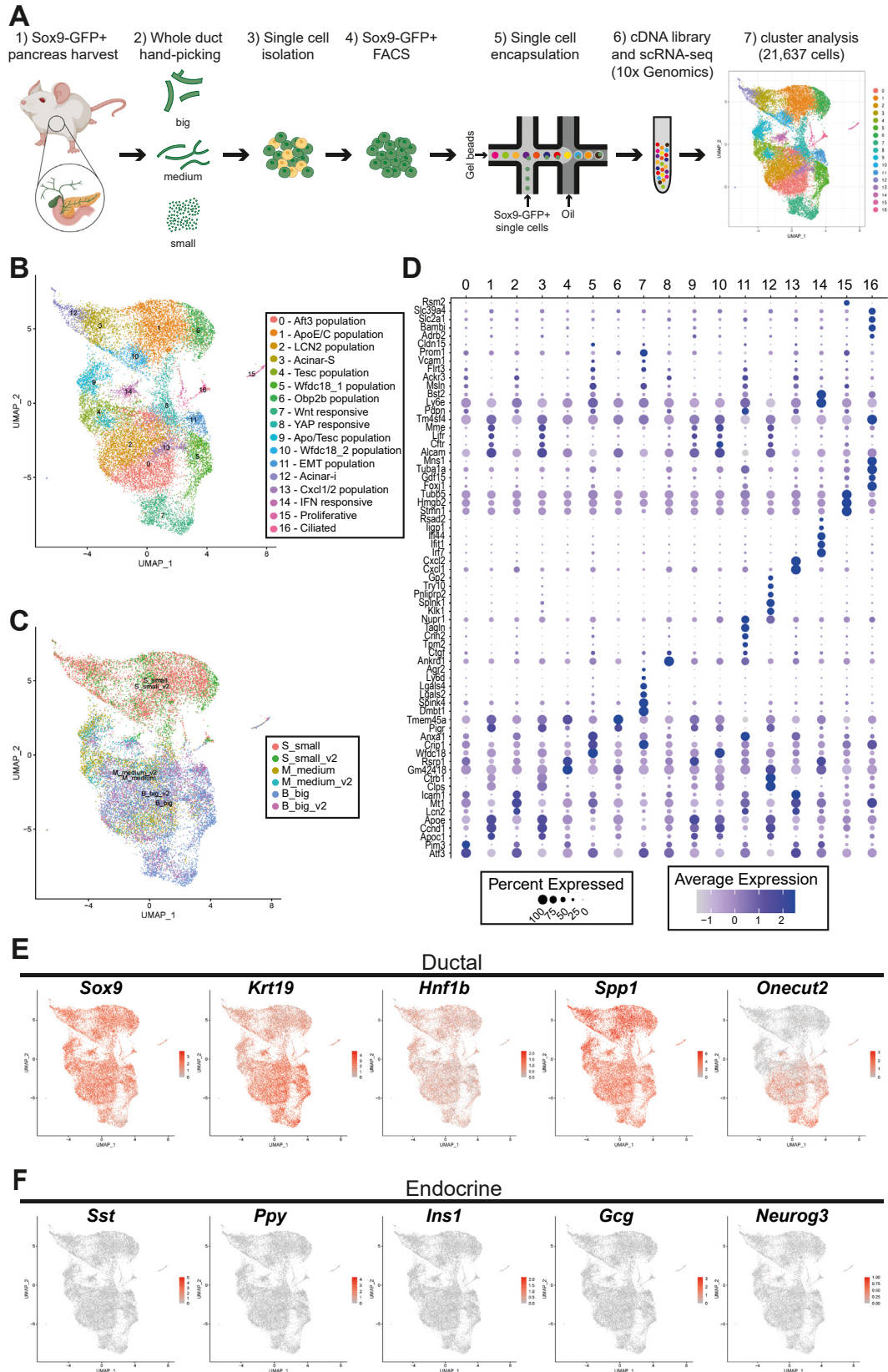


Figure 3. scRNA-seq identifies 15 subtypes of ductal cells. (A) Schematic representation of the experimental workflow for scRNA-seq (created with BioRender.com). (B) UMAP of 21,637 Sox9:eGFP⁺ colored after clustering analysis. (C) UMAP with samples clustered and colored by the size of the ducts and experimental replicates. (D) Dot plot of cell type-enriched genes per clusters. (E) UMAP plots showing the expression of pancreatic ductal markers. (F) UMAP plot showing the expression of pancreatic endocrine markers: *Gcg*, *Ins1*, *Sst*, *Ppy*, and *Neurog3*. cDNA, complementary DNA.

which has recently been reported as a regulator of cancer progression.³⁰

Clusters derived from big ducts are characterized by the expression of previously unidentified ductal markers. Cluster 2 (Lcn2 population) is characterized by *Lcn2* and *Icam1* expression. Both have increased expression in pancreatitis, pancreatic intraepithelial neoplasia (PanIN), and PDAC.^{31,32} Cluster 5 (*Wfdc18_1* population), is characterized by high expression of *Wfdc18*, like cluster 10. Interestingly, cluster 7 (Wnt-responsive population) expresses many markers shared with progenitors in other tissues, including *Olfm4*, *Ly6D*, *Agr2*, and *Hes1*; therefore displaying a progenitor-like transcriptome similar to intestine³³ and prostate,³⁴ including Wnt-responsive genes (*Ascl2*, *Rnf43*, and *Znrf3*). Cluster 13 (*Cxcl1/2* population) is characterized by high expression of *Cxcl1* and *Cxcl2*.

Several clusters were derived from medium-big ducts. Cluster 0 (*Atf3* population) expresses high levels of *Atf3*. *Atf3* deletion in acinar cells decreased pancreatitis-induced ADM, PanIN formation, and PDAC.³⁵ Cluster 9 (*Apo/Tesc* population) shares most markers with clusters 4 or 1. Cluster 11 (epithelial-to-mesenchymal transition [EMT] population) is characterized by the expression of *Tagln*, *Tpm2*, and *Tpm1*, which have been identified as markers of myofibroblast-like cancer-associated fibroblasts in PDAC,³⁶ although these cells maintain the expression of ductal cells markers, thus suggesting an epithelial-mesenchymal transition state.

Finally, among the clusters composed of mixed compartments, cluster 8 (YAP-responsive population) is highly enriched in YAP target genes, including *Ankrd1*, *Ctgf*, and *Cyr61*. Hippo-signaling has been found to play key roles in pancreas progenitor maintenance, renewal, proliferation, and differentiation.³⁷ Unexpectedly, cluster 14 (interferon [IFN]-responsive population) is highly enriched in antigen-presenting and IFN response genes (*Isg15*, *Ifitm3*, *Ifi1712a*, and *Irf7*) that have recently been related to a ductal population enriched in islets of type 1 diabetes (T1D) patients that could play a role in immune eviction.³⁸ Cluster 15 (proliferative population) represents a subset of cycling ductal cells. Finally, cluster 16 (ciliated population) is characterized by high expression of motile cilia markers, such as *Spag16* and *Foxj1*.

Wnt-Responsive Population Is Located in Big Ducts and Pancreatic Ductal Glands

Gene Ontology analysis showed many biological processes shared by several clusters, such as tissue development, positive regulation of cellular processes, and cellular respiration (Supplementary Figure 5 and Supplementary Table 5). Remarkably, some clusters display unique terms, such as cluster 14 (IFN-responsive population), enriched in immune response and cellular response to IFN pathways. Clusters 5 and 11 (*Wfdc18_1* population and EMT population, respectively) were enriched in terms related to cell migration and differentiation. Cluster 15 (proliferative population) was enriched in mitotic processes and RNA splicing. Cluster 16 (ciliated population) was enriched in cilium assembling, docking, and transport (Figure 4B and

Supplementary Figure 5). Thus, our scRNA-seq results show ductal heterogeneity and highlight previously unidentified ductal populations that could play different roles in pancreatic pathogenesis and regeneration.

Interestingly, the Wnt-responsive population was enriched in biological processes related to ribosome biogenesis and translation (Figure 4B), which are linked to stemness, especially in quiescent stem cells.³⁹ When analyzing Kyoto Encyclopedia of Genes and Genomes pathways with genes overexpressed ≥ 1.5 -fold in this population, we observed an enrichment of signaling pathways regulating stem cell pluripotency (Figure 5B and Supplementary Table 6). At the same time, CellMarker analysis⁴¹ showed high similarities with intestinal and basal stem cells and side population (Figure 5A and Supplementary Table 6), thus suggesting a stem-like phenotype of this population. Many classical markers expressed by *Lgr5* intestinal stem cells, but not *Lgr5* (Supplementary Figure 3D), were expressed by the Wnt-responsive population (Figure 5C). This population also expresses markers previously identified in the common biliary duct, like *Dmbt1* and *Ly6D*.⁴² These results suggest that the Wnt-responsive population resembles a population located in the common biliary duct. Interestingly, staining for Wnt-responsive population markers (*Ly6D*, *Agr2*, or *Olfm4*) showed its expression only in budding/outpouching structures in the main duct, named pancreatic ductal glands (PDGs)⁴³ (Figure 5D). The main duct was manually dissected to ensure that the glands were in the main duct and not in the common pancreatobiliary duct (Supplementary Figure 2E). Interestingly, PDGs have been suggested to be niche compartments both in mouse and human pancreas, displaying progenitor capacities and playing a role in the regeneration of exocrine pathologies.^{43,44}

In Situ Characterization of Ductal Populations in Adult Pancreatic Tissue and Injury Models

To further validate the correlation of scRNA-seq data at the protein level, we characterized the expression of other populations' specific markers in situ by immunofluorescence multiplexing using MACSima technology and by immunohistochemistry in healthy pancreatic tissue (Figure 5D and Supplementary Figure 6A). Significantly, we confirmed protein expression of most of the cluster-specific markers (Figure 5E and Supplementary Figure 6), showing an enrichment correlation with our scRNA-seq data for 71.4% (15 out of 21) of the markers (Figure 5E and Supplementary Figure 6B). Next, we characterized the expression of specific markers in CP and observed that *Olfm4*, *Agr2*, *AnxA3*, and *Isg15* are heterogeneously expressed in ADM regions in CP samples, suggesting a putative role of the Wnt-responsive, EMT and IFN-responsive populations in pancreatitis pathogenesis (Figure 6A).

In recent years, several laboratories have described acinar and ductal cells as origins of PDAC.^{4,21,45,46} Ductal-derived PDACs, characterized by the expression of *Agr2*⁴⁷ or IFN signaling-related genes,⁴⁵ are more aggressive and have a poorer outcome. Interestingly, the Wnt-responsive

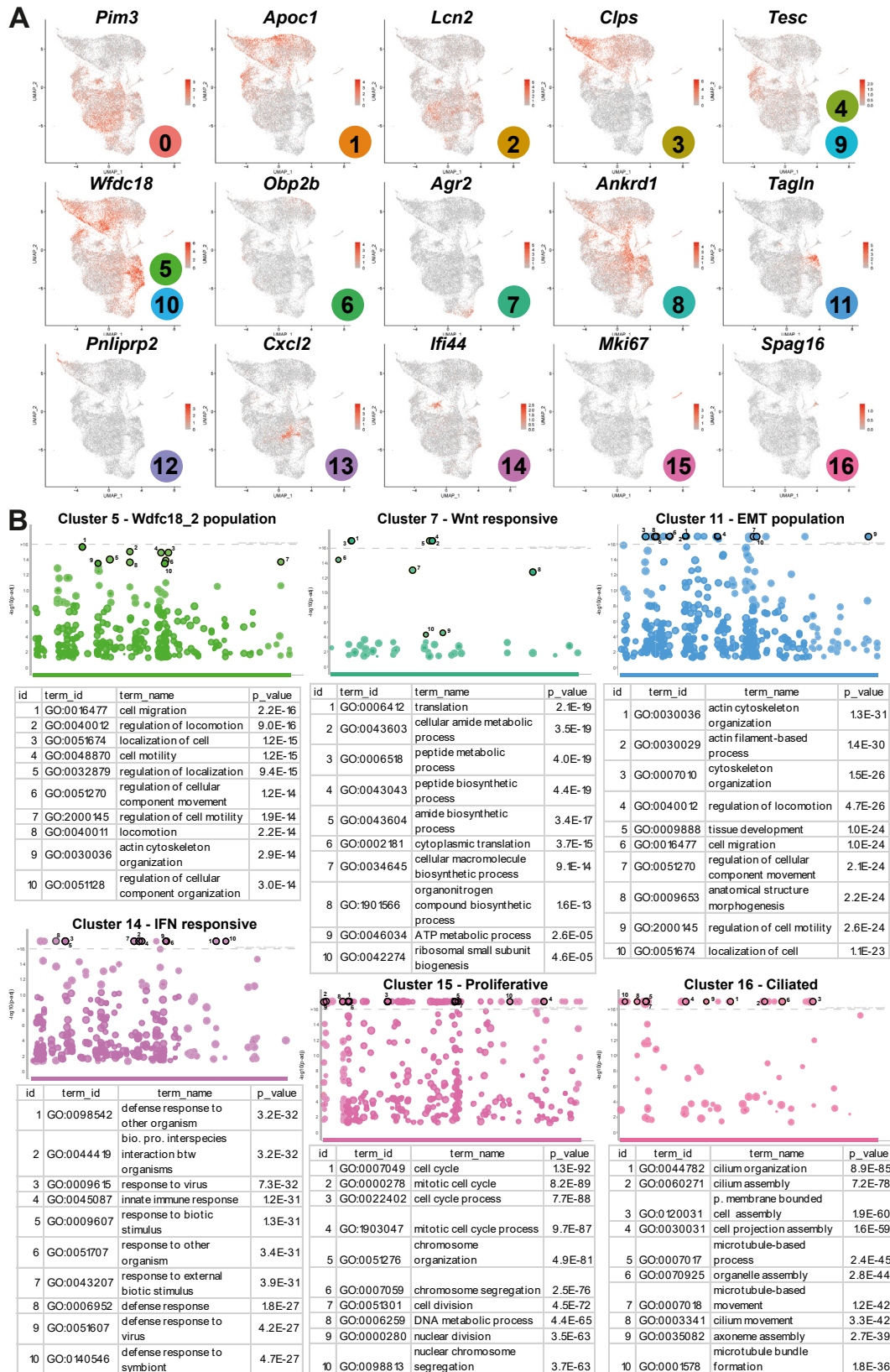
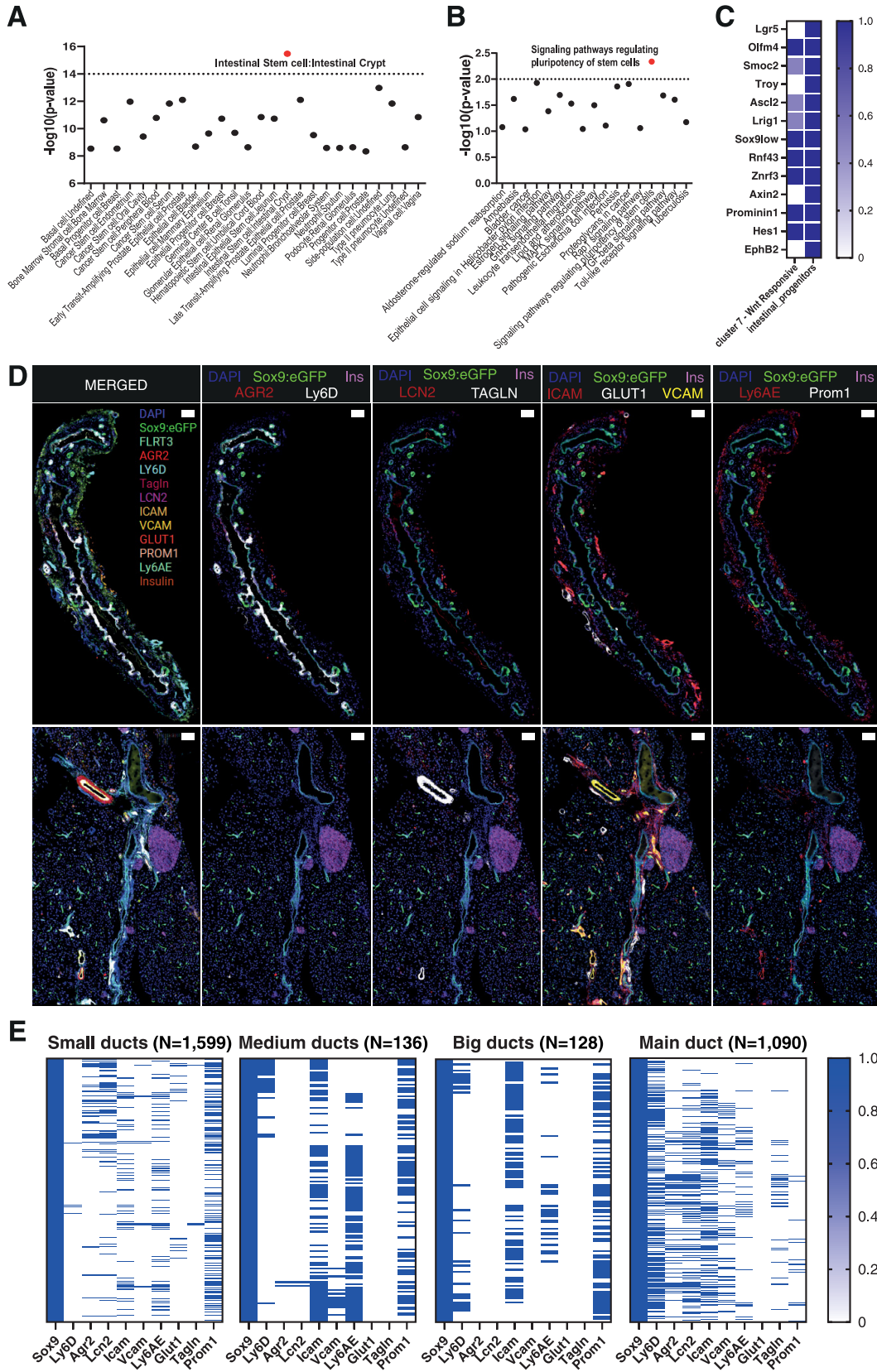


Figure 4. Cluster-specific markers and Gene Ontology analysis of novel ductal populations. (A) UMAP plots of cluster-specific markers for each identified ductal population. (B) Gene Ontology analysis plots for clusters 5, 7, 11, and 14–16, with the top 10 significant Gene Ontology terms.

population is characterized by the expression of *Agr2* and *Olfm4* and the IFN-responsive population by IFN-related genes, such as *Isg15* and *Bst2*. Thus, we characterized the

expression of those markers in mouse PDAC samples, either in tumors where *Kras* mutation and *P53* deletion are induced by *Pdx1-Cre* (progenitor derived, *KPC⁴⁸*) or by



HNF1bCreERT2 (ductal derived, HPC^{21,46}) system. In Pdx1-derived tumors, we observed scattered expression of *Agr2*, *Olfm4*, *AnxA3*, and *Isg15* in the tumor, ADM, and PanIN lesions. In ductal-derived tumors, we observed 2 different patterns in PanINs: uniformly expressing PanINs and PanINs lacking marker expression (Figure 6A). Further comparison of our data to single-cell data of preinvasive lesions in mouse PDAC samples⁴⁹ showed that the transcriptional signatures of big duct-derived populations, including the Wnt-responsive and EMT populations (and, to a lesser extent, the IFN-responsive population) were more highly expressed in ductal and metaplastic cells in tumor samples, again suggesting a role of these ductal cells in tumorigenesis (Supplementary Figure 7).

Interestingly, specific markers from the Wnt-responsive, IFN-responsive, and EMT populations had higher outcome predictive values in human samples than genes in other populations, such as the *Obp2b* population, *Cxcl1/2* population, *Lcn2* population, or *Tesc* population (Supplementary Figure 8A). Further characterization of Wnt-responsive, IFN-responsive, and EMT population markers in human PDAC samples shows inter- and intratumor sample heterogeneity (Figure 6B). Moreover, we observed that type 2 “malignant” ductal cells described by Peng et al⁵⁰ that were linked to poor prognosis had a transcriptional profile enriched for the markers from Wnt-responsive, IFN-responsive and EMT populations (Supplementary Figure 8B–D), thus supporting our hypothesis that those populations could play an essential role in PDAC development.

Isolation of Newly Identified Populations and In Vitro Characterization of Exocrine/Endocrine Differentiation Capacity

To further study newly defined populations in organoid cultures, we intersected our scRNA-seq data with the human protein atlas data on membrane proteins⁵¹ and identified antibodies against extracellular epitopes of these proteins. Isolation of ductal compartments followed by antibody staining of specific surface markers confirmed the enrichment of the ductal populations in the compartments identified by scRNA-seq in 10 out of the 15 markers analyzed (Figure 7A and Supplementary Figure 9A). We isolated Ly6D⁺ cells (Wnt-responsive population), *Bambi*⁺ cells (ciliated population), *Bst2*⁺ and *Ly6A/E*⁺ cells (INF-responsive population and cells from medium/big ducts), *Vcam1*⁺ cells (*Wfdc18_1* population), *Icam1*⁺ cells (*Atf3*, *ApoE/C*, and *Cxcl1/2* populations), *Ackr3*⁺ and *Flrt3*⁺ cells (medium-big duct-derived clusters), and *CD166/Alcam*⁺

cells (panductal). *CD133/prominin* was selected as the stem cell marker already used to test ductal cell stemness (reviewed by Casamitjana et al⁵²). *Glut1/Slc2a1* was used to isolate a fraction of ductal cells while not defining a cluster. Finally, *Mme* was used to enrich for small ductal cells, although the expression pattern observed by FACS did not correlate with scRNA-seq expression (Figure 7A and Supplementary Figure 9A).

The organoid formation capacity of the isolated populations based on *Sox9:eGFP* expression and specific surface markers was interrogated by plating the same cell density (Figure 7B and C). All isolated populations formed organoids, although at different efficiencies. The populations with higher organoid formation efficiency were derived from medium-big ducts, including *Ly6D* (20.05% ± 2.25%), *Icam1* (16.24% ± 7.98%), *Glut1* (13.89% ± 3.55%), *Vcam1* (10.38% ± 3.55%), *Ly6A/E* (7.95% ± 2.34%), *Flrt3* (12.43% ± 5.88%), and *Bambi* (10.28% ± 8.87%). Some of the isolated populations displayed low organoid formation capacity below the 7.93% observed in big ducts (Figure 1I), including *prominin*, *Ackr3* and *Mme* (7.43% ± 3.48%, 3.04% ± 2.3%, and 7.65% ± 8.39%, respectively). We also quantified organoid size (Supplementary Figure 8B), showing different growth capacities. Notably, organoid heterogeneity was highly reduced based on ductal markers (Figure 7D). Only populations with higher organoid formation efficiency than big ducts were further analyzed.

In vitro differentiation of the isolated populations into the endocrine lineages showed that *Bambi*⁺ cells display a significant capacity to differentiate into endocrine progenitors—an up to 50-fold increase of *Neurog3* expression vs control organoids (53.49 ± 19.89) (Figure 7E). The remaining populations display increased capacity for differentiation into *Neurog3*-expressing cells when compared to big-duct-derived organoids, although they do not reach statistical significance. Surprisingly, *Bambi*-derived organoids did not display a high capacity of differentiation into endocrine lineages based on *Ins*, *Gcg*, and *Sst* mRNA expression; instead, *Flrt3*-derived organoids display higher capacity of differentiation into all endocrine lineages (Figure 7E). Curiously, *Ly6D*-derived organoids show higher capacity to differentiate into acinar cells based on *Amylase* expression (Supplementary Figure 9C).

Discussion

Pancreatic heterogeneity, at single-cell resolution, has been mainly exploited to study pancreatic endocrine cells; thus, ductal heterogeneity has not been deeply analyzed in

Figure 5. Detection of novel ductal markers in healthy pancreatic tissue, including the Wnt-responsive population in PDGs. (A) Plots showing Enrichr analysis⁴⁰ for the Wnt-responsive population in CellMarker_Augmented [hits = $-\log(P \text{ value}) > 8$] and (B) KEGG2021 [hits = $-\log(P \text{ value}) > 1$]. (C) Gene expression comparison between the Wnt-responsive population and intestinal progenitors.³³ (D) Multiplex immunofluorescence images of the main duct, including PDGs, and whole pancreas section using MACSima Imaging Cyclic Staining technology of newly identified populations: *Tagln* (EMT population); *Ly6D* and *Agr2* (Wnt-responsive population); *Glut1* (some ductal cells); *Lcn2* and *Icam* (*Lcn2* population); *Vcam* (*Wfdc18_1* population); *Ly6A/E* (INF population); and *Prominin1* expressed in most ductal cells and lineage markers, *Insulin* and *Sox9*. Scale bar, 100 μm . (E) Heatmap plot quantifying specific marker expression of novel ductal populations (blue, expression; white, absence of expression).

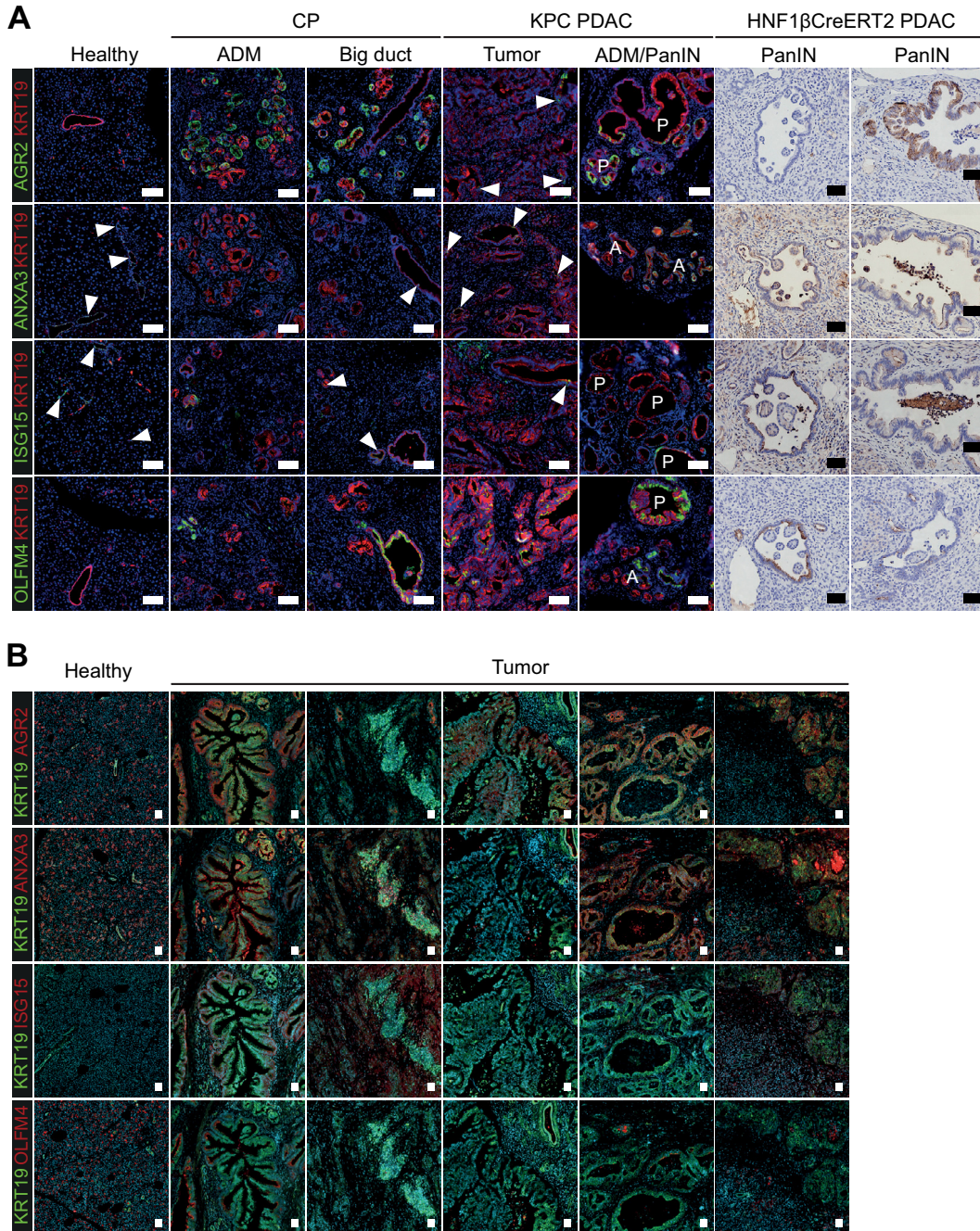


Figure 6. Characterization of ductal populations in adult pancreas, CP, and PDAC. (A) Representative immunofluorescence/immunohistochemistry images of healthy, CP, and PDAC samples from KPC and HPC mice. Staining of population markers Agr2 and Olfm4 (Wnt-responsive population), Isg15 (INF-responsive population), and Anxa3 (EMT population) are in green, and pancreatic marker Krt19 is in red. Representative images of ADM (A), tumor, and PanINs (P) are shown per every marker analyzed. Arrowheads indicate coexpression of population markers and Krt19. Scale bar, 50 μm. (B) Representative immunofluorescence images of consecutive sections of 5 independent human PDAC samples stained with the same population-specific markers detected in red and pancreatic marker Krt19 in green, showing intra- and intertumor heterogeneity expression. Scale bar, 50 μm.

mice or humans. The first glimpse of such heterogeneity was highlighted in recent publications^{16,17}; although these studies do not include cells from all ductal compartments, only a couple of thousand cells were analyzed. For the first time, we have generated a cell atlas of the entire murine pancreatic ductal epithelium from the tip (CACs) up to the

main duct, including PDGs. Our results have uncovered an unprecedented level of heterogeneity in the ductal compartment. Interestingly, recent work by Fasolino et al³⁸ discovered a subset of ductal cells that acquires a signature of tolerogenic dendritic cells in an attempt at immune suppression in T1D donors, highlighting a novel role of

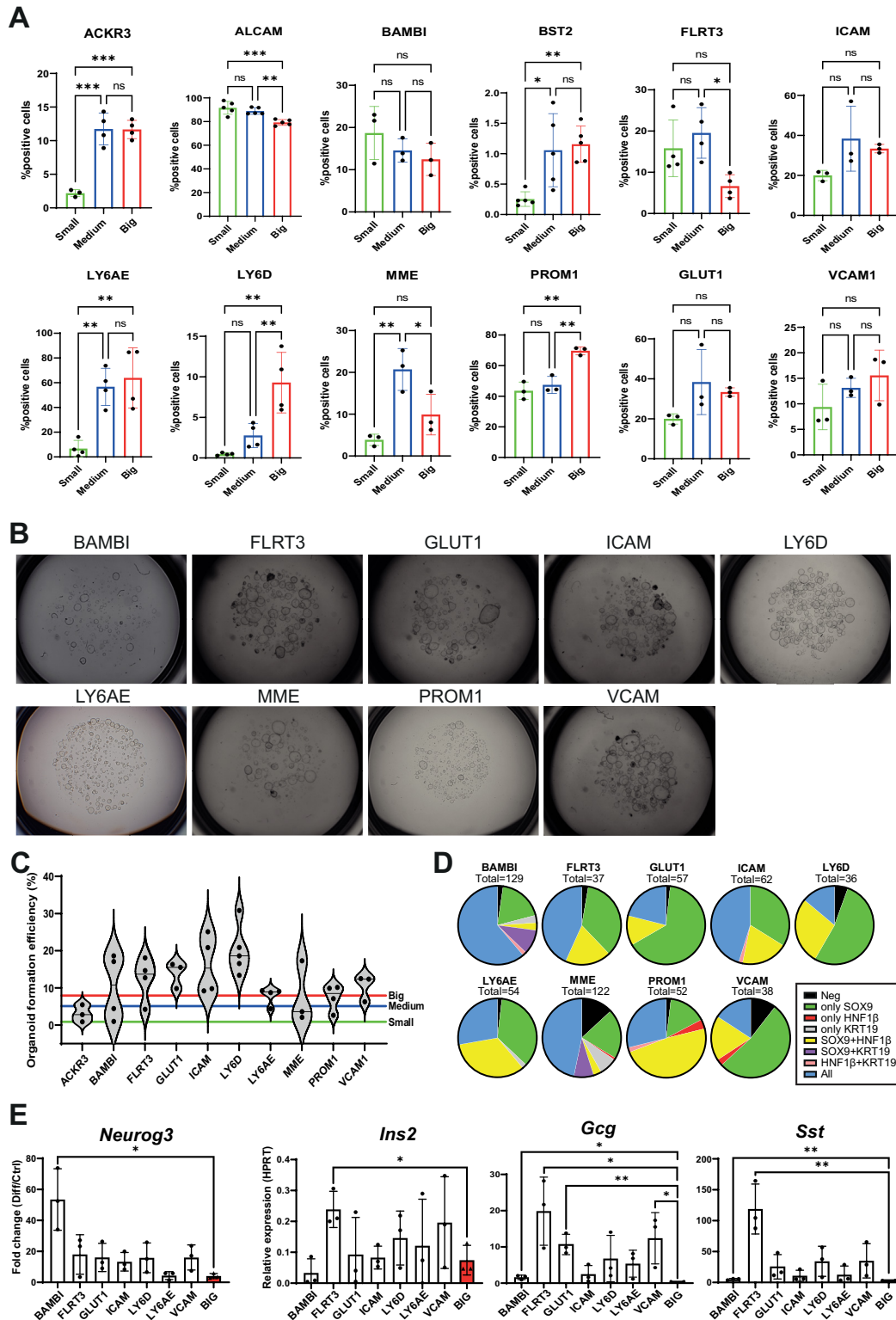


Figure 7. Isolation of newly identified populations and in vitro characterization in organoid cultures upon endocrine differentiation. (A) Bar plots showing quantification of ductal population distribution in small, medium, and big enriched ductal fractions by FACS (1-way analysis of variance, Tukey’s post hoc test, N = 3–5). (B) Representative images of organoid formation efficiency upon 10-day cultures. (C) Violin plot showing quantification of organoid formation efficiency (N = 3–5) and population mean. Colored lines indicate the mean of organoid formation in big (red), medium (blue), and small (green) duct-derived organoids. (D) Pie charts showing the quantification of ductal marker expression by antibody staining (Sox9, Hnf1b, and Krt19) in population-derived organoids. (E) qPCR analysis on population-derived organoids upon differentiation for *Neurog3*, *Ins2*, *Gcg*, and *Sst* (Student *t* test vs big [red], N = 3).

ductal cells in T1D pathogenesis. Interestingly, our scRNA-seq analysis demonstrated the presence of this population scattered through the ductal epithelium. Thus, further investigations are needed to understand the role of this population in the development and pathophysiology of diabetes or exocrine diseases.

We have defined an in vitro protocol to efficiently induce differentiation of organoids into Neurog3⁺ progenitors and, to a lesser extent, into hormone-producing cells. Interestingly, bigger ducts and derived organoids express lower levels of *Spp1*; thus, our results are in concordance with the recent observations demonstrating that inhibition of *Spp1* in ductal cells induces insulin expression in vitro.¹⁷ Our scRNA-seq data reflect the coexistence of 15 ductal populations, some of which were not previously identified,^{16,17} and demonstrated functional differences within the ductal epithelia. The likelihood of a pool of dedicated progenitors in the adult pancreas is low; thus β -cell neogenesis has been controversial. Most lineage tracing studies, using panductal-specific Cre lines,¹¹ did not find a quantifiable and physiologically relevant contribution of β -cell neogenesis from ducts. These previous results do not disprove the plasticity of ductal cells in vitro, in organoid cultures, as we have demonstrated here, showing that different ductal compartments behave differently in organoid cultures at various levels, from organoid formation to endocrine/exocrine differentiation.

We further showed that, upon FACS isolation of novel populations, Bambi, Flrt3, Glut1, Icam1, Ly6D, and Vcam ductal cells display >10% organoid formation efficiency, although organoid formation did not correlate with an increased endocrine differentiation potential, at least under the same media conditions. Surprisingly, organoids derived from the Bambi ciliated population display high differentiation capacity toward endocrine progenitors but not hormone-producing cells. Intriguingly, Flrt3-derived organoids show high efficiency of differentiation into hormone-expressing cells. Flrt3 has been found to be expressed in pancreatic multipotent progenitors at E9.5.⁵³ Strikingly, the Wnt-responsive population located in PDGs displays stemness features, showing high exocrine regenerative capacity.

Future manipulations to promote β -cell differentiation from organoids are needed to develop efficient protocols. We have used standardized media for organoid formation and differentiation; thus, further investigation on whether signaling cues required to differentiate novel ductal populations into the endocrine/exocrine lineages differ between them is necessary. Nevertheless, our results demonstrated a putative role of novel ductal populations in endocrine and exocrine regeneration. Moreover, new lineage-tracing models will be critical to further investigate the role in pancreas regeneration of the Wnt-responsive and Flrt3 populations.

Our results suggest that newly identified populations might play a role in pancreatic exocrine pathogenesis because the expression of their markers increases in ADM regions in CP. In addition, recent reports highlighted acinar and ductal cells of origin of PDAC. Interestingly, our analysis

showed the existence of 3 ductal populations—the Wnt-responsive, IFN-responsive, and EMT populations—showing higher outcome predictive values in human PDAC samples than genes in other populations. Significantly, transcriptional comparison with scRNA-seq in human PDAC samples correlates with an enrichment of the populations mentioned in tumor samples. Thus, our results suggest that novel ductal populations could play different roles in the pathophysiology of exocrine pancreatic diseases and different ductal cells of origin of PDAC. This hypothesis requires further investigation with novel lineage-tracing models to rule out a simple reactivation of population markers, understand their function in different exocrine disease states, and increase our understanding of the biology and PDAC heterogeneity. If uncovered, it would be critical to investigate the differences in tumor development and biomarkers according to a ductal cell of origin with implications in tumor stratification of PDAC patients according to ductal markers that may affect the prediction outcomes and allow for the identification of novel therapeutic targets to design a personalized medicine strategy.

Considering our discovery of previously unidentified ductal populations, we unmasked the potential roles of specific ductal populations in endocrine/exocrine regeneration and pathogenesis. Therefore, our results compel the need to reinterpret the cellular pathogenesis of pancreatic diseases and to revisit previous lineage-tracing experiments using panductal markers by generating new tracing tools to study ductal-specific populations and investigate their regenerative potential and their role in exocrine pathogenesis in vivo.

Supplementary Material

Note: To access the supplementary material accompanying this article, visit the online version of *Gastroenterology* at www.gastrojournal.org, and at <https://doi.org/10.1053/j.gastro.2024.06.008>.

References

1. Grapin-Botton A. Ductal cells of the pancreas. *Int J Biochem Cell Biol* 2005;37:504–510.
2. Cao D, Maitra A, Saavedra JA, et al. Expression of novel markers of pancreatic ductal adenocarcinoma in pancreatic nonductal neoplasms: additional evidence of different genetic pathways. *Mod Pathol* 2005;18:752–761.
3. Busnardo AC, DiDio LJ, Tidrick RT, et al. History of the pancreas. *Am J Surg* 1983;146:539–550.
4. Lee AYL, Dubois CL, Sarai K, et al. Cell of origin affects tumour development and phenotype in pancreatic ductal adenocarcinoma. *Gut* 2019;68:487–498.
5. McCarthy N, Kraiczky J, Shivdasani RA. Cellular and molecular architecture of the intestinal stem cell niche. *Nat Cell Biol* 2020;22:1033–1041.
6. Guiu J, Hannezo E, Yui S, et al. Tracing the origin of adult intestinal stem cells. *Nature* 2019;570:107–111.
7. Bonner-Weir S, Baxter LA, Schuppin GT, et al. A second pathway for regeneration of adult exocrine and

- endocrine pancreas. A possible recapitulation of embryonic development. *Diabetes* 1993;42:1715–1720.
8. Yoneda S, Uno S, Iwahashi H, et al. Predominance of β -cell neogenesis rather than replication in humans with an impaired glucose tolerance and newly diagnosed diabetes. *J Clin Endocrinol Metab* 2013;98:2053–2061.
 9. Kopp JL, Dubois CL, Schaffer AE, et al. Sox9⁺ ductal cells are multipotent progenitors throughout development but do not produce new endocrine cells in the normal or injured adult pancreas. *Development* 2011;138:653–665.
 10. Delaspre F, Beer RL, Rovira M, et al. Centroacinar cells are progenitors that contribute to endocrine pancreas regeneration. *Diabetes* 2015;64:3499–3509.
 11. Afelik S, Rovira M. Pancreatic β -cell regeneration: facultative or dedicated progenitors? *Mol Cell Endocrinol* 2017;445:85–94.
 12. Magenheimer J, Maestro MA, Sharon N, et al. Matters arising: insufficient evidence that pancreatic β cells are derived from adult ductal Neurog3-expressing progenitors. *Cell Stem Cell* 2023;30:488–497.e3.
 13. Huch M, Bonfanti P, Boj SF, et al. Unlimited in vitro expansion of adult bi-potent pancreas progenitors through the Lgr5/R-spondin axis. *EMBO J* 2013;32:2708–2721.
 14. Clevers H. Modeling development and disease with organoids. *Cell* 2016;165:1586–1597.
 15. Wang YJ, Kaestner KH. Single-cell RNA-seq of the pancreatic islets—a promise not yet fulfilled? *Cell Metab* 2019;29:539–544.
 16. Qadir MMF, Álvarez-Cubela S, Klein D, et al. Single-cell resolution analysis of the human pancreatic ductal progenitor cell niche. *Proc Natl Acad Sci U S A* 2020;117:10876–10887.
 17. Hendley AM, Rao AA, Leonhardt L, et al. Single-cell transcriptome analysis defines heterogeneity of the murine pancreatic ductal tree. *Elife* 2021;10:e67776.
 18. Tosti L, Hang Y, Debnath O, et al. Single-nucleus and in situ RNA-sequencing studies reveal cell topographies in the human pancreas. *Gastroenterology* 2021;160:1330–1344.e11.
 19. Gong S, Zheng C, Doughty ML, et al. A gene expression atlas of the central nervous system based on bacterial artificial chromosomes. *Nature* 2003;425:917–925.
 20. Grimont A, Pinho AV, Cowley MJ, et al. SOX9 regulates ERBB signalling in pancreatic cancer development. *Gut* 2015;64:1790–1799.
 21. Singh K, Pruski M, Bland R, et al. *Kras* mutation rate precisely orchestrates ductal derived pancreatic intraepithelial neoplasia and pancreatic cancer. *Lab Invest* 2021;101:177–192.
 22. Rovira M, Scott S-G, Liss AS, et al. Isolation and characterization of centroacinar/terminal ductal progenitor cells in adult mouse pancreas. *Proc Natl Acad Sci U S A* 2010;107:75–80.
 23. Yong HJ, Xie G, Liu C, et al. Gene signatures of NEUROGENIN3⁺ endocrine progenitor cells in the human pancreas. *Front Endocrinol (Lausanne)* 2021;12:736286.
 24. Lacazette E, Gachon AM, Pitiot G. A novel human odorant-binding protein gene family resulting from genomic duplicons at 9q34: differential expression in the oral and genital spheres. *Hum Mol Genet* 2000;9:289–301.
 25. Takano S, Yoshitomi H, Togawa A, et al. Apolipoprotein C-1 maintains cell survival by preventing from apoptosis in pancreatic cancer cells. *Oncogene* 2008;27:2810–2822.
 26. Ioannou M, Serafimidis I, Arnes L, et al. ALDH1B1 is a potential stem/progenitor marker for multiple pancreas progenitor pools. *Dev Biol* 2013;374:153–163.
 27. Hosein AN, Huang H, Wang Z, et al. Cellular heterogeneity during mouse pancreatic ductal adenocarcinoma progression at single-cell resolution. *JCI Insight* 2019;5:e129212.
 28. Wang J, Kilic G, Aydin M, et al. Prox1 activity controls pancreas morphogenesis and participates in the production of “secondary transition” pancreatic endocrine cells. *Dev Biol* 2005;286:182–194.
 29. Gibson-Corley KN, Meyerholz DK, Engelhardt JF. Pancreatic pathophysiology in cystic fibrosis. *J Pathol* 2016;238:311–320.
 30. Lee JH, Choi SI, Kim RK, et al. Tescalcin/c-Src/IGF1R β -mediated STAT3 activation enhances cancer stemness and radioresistant properties through ALDH1. *Sci Rep* 2018;8:10711.
 31. Leung L, Radulovich N, Zhu CQ, et al. Lipocalin2 promotes invasion, tumorigenicity and gemcitabine resistance in pancreatic ductal adenocarcinoma. *PLoS One* 2012;7:e46677.
 32. Liou GY, Döppler H, Necela B, et al. Mutant KRAS-induced expression of ICAM-1 in pancreatic acinar cells causes attraction of macrophages to expedite the formation of precancerous lesions. *Cancer Discov* 2015;5:52–63.
 33. Muñoz J, Stange DE, Schepers AG, et al. The Lgr5 intestinal stem cell signature: robust expression of proposed quiescent ‘+4’ cell markers. *EMBO J* 2012;31:3079–3091.
 34. Barros-Silva JD, Linn DE, Steiner I, et al. Single-cell analysis identifies LY6D as a marker linking castration-resistant prostate luminal cells to prostate progenitors and cancer. *Cell Rep* 2018;25:3504–3518.e6.
 35. Azizi N, Toma J, Martin M, et al. Loss of activating transcription factor 3 prevents KRAS-mediated pancreatic cancer. *Oncogene* 2021;40:3118–3135.
 36. Elyada E, Bolisetty M, Laise P, et al. Cross-species single-cell analysis of pancreatic ductal adenocarcinoma reveals antigen-presenting cancer-associated fibroblasts. *Cancer Discov* 2019;9:1102–1123.
 37. Cebola I, Rodríguez-Seguí SA, Cho CH, et al. TEAD and YAP regulate the enhancer network of human embryonic pancreatic progenitors. *Nat Cell Biol* 2015;17:615–626.
 38. Fasolino M, Schwartz GW, Patil AR, et al. Single-cell multi-omics analysis of human pancreatic islets reveals novel cellular states in type 1 diabetes. *Nat Metab* 2022;4:284–299.
 39. Sharifi S, da Costa HFR, Bierhoff H. The circuitry between ribosome biogenesis and translation in stem cell function and ageing. *Mech Ageing Dev* 2020;189:111282.

40. Kuleshov MV, Jones MR, Rouillard AD, et al. Enrichr: a comprehensive gene set enrichment analysis web server 2016 update. *Nucleic Acids Res* 2016;44:W90–W97.
41. Zhang X, Lan Y, Xu J, et al. CellMarker: a manually curated resource of cell markers in human and mouse. *Nucleic Acids Res* 2019;47:D721–D728.
42. Pepe-Mooney BJ, Dill MT, Alemany A, et al. Single-cell analysis of the liver epithelium reveals dynamic heterogeneity and an essential role for YAP in homeostasis and regeneration. *Cell Stem Cell* 2019;25:23–38.e8.
43. Yamaguchi J, Liss AS, Sontheimer A, et al. Pancreatic duct glands (PDGs) are a progenitor compartment responsible for pancreatic ductal epithelial repair. *Stem Cell Res* 2015;15:190–202.
44. Strobel O, Rosow DE, Rakhlin EY, et al. Pancreatic duct glands are distinct ductal compartments that react to chronic injury and mediate Shh-induced metaplasia. *Gastroenterology* 2010;138:1166–1177.
45. Espinet E, Gu Z, Imbusch CD, et al. Aggressive PDACs show hypomethylation of repetitive elements and the execution of an intrinsic IFN program linked to a ductal cell of origin. *Cancer Discov* 2021;11:638–659.
46. Bailey JM, Hendley AM, Lafaro KJ, et al. p53 mutations cooperate with oncogenic Kras to promote adenocarcinoma from pancreatic ductal cells. *Oncogene* 2016;35:4282–4288.
47. Ferreira RMM, Sancho R, Messal HA, et al. Duct- and acinar-derived pancreatic ductal adenocarcinomas show distinct tumor progression and marker expression. *Cell Rep* 2017;21:966–978.
48. Hingorani SR, Wang L, Multani AS, et al. *Trp53R172H* and *KrasG12D* cooperate to promote chromosomal instability and widely metastatic pancreatic ductal adenocarcinoma in mice. *Cancer Cell* 2005;7:469–483.
49. Schlesinger Y, Yosefov-Levi O, Kolodkin-Gal D, et al. Single-cell transcriptomes of pancreatic preinvasive lesions and cancer reveal acinar metaplastic cells' heterogeneity. *Nat Commun* 2020;11:4516.
50. Peng J, Sun BF, Chen CY, et al. Single-cell RNA-seq highlights intra-tumoral heterogeneity and malignant progression in pancreatic ductal adenocarcinoma. *Cell Res* 2019;29:725–738.
51. Thul PJ, Åkesson L, Wiking M, et al. A subcellular map of the human proteome. *Science* 2017;356:eaal3321.
52. Casamitjana J, Espinet E, Rovira M. Pancreatic organoids for regenerative medicine and cancer research. *Front Cell Dev Biol* 2022;10:886153.
53. Willnow D, Benary U, Margineanu A, et al. Quantitative lineage analysis identifies a hepato-pancreato-biliary progenitor niche. *Nature* 2021;597:87–91.

Received August 24, 2023. Accepted June 7, 2024.

Correspondence

Address correspondence to: Meritxell Rovira, PhD, University of Barcelona (UB), School of Medicine, Department of Physiological Science, Pavelló de Govern, Carrer Feixa Llarga, s/n, 08907, L'Hospitalet de Llobregat, Barcelona, Spain. e-mail: mrovira@idibell.cat or meritxell.rovira@ub.edu.

Acknowledgments

The authors thank IDIBELL's animal facility and mouse laboratory unit for the housing and maintenance of the Sox9:eGFP line; IDIBELL's flow cytometry facility, especially J. M. Andrés Vaquero; and IDIBELL's histology facility, especially Lola Mulero and Jose Llamas, and imaging facility, especially Joan Repullès and Saïoa Mendizuri. The authors are also grateful for the service provided by Visual & Spatial Tissue Analysis (<https://vsta.research.vub.be>). Drawings were created with BioRender.com.

CRedit Authorship Contributions

Ángel Fernández, MSc (Formal analysis: Lead; Investigation: Equal; Methodology: Equal; Validation: Lead; Writing – original draft: Supporting)
 Joan Casamitjana, PhD (Data curation: Equal; Formal analysis: Equal; Investigation: Equal; Methodology: Equal; Validation: Equal; Visualization: Equal; Writing – original draft: Supporting)
 Adrián Holguín-Horcajo, MSc (Investigation: Equal; Methodology: Equal; Validation: Equal)
 Katarina Coolens, MSc (Investigation: Supporting; Methodology: Supporting; Validation: Supporting)
 Loris Mularoni, PhD (Data curation: Equal; Formal analysis: Equal; Resources: Equal)
 Li Guo, PhD (Formal analysis: Supporting)
 Olga Hartwig, PhD (Methodology: Supporting; Validation: Supporting)
 Tim Düking, PhD (Methodology: Supporting; Validation: Supporting)
 Noemi Vidal, MD (Resources: Supporting)
 Lincoln N. Strickland, MSc (Validation: Supporting)
 Lorenzo Pasquali, MD, PhD (Supervision: Supporting; Writing – original draft: Supporting)
 Jennifer M. Bailey-Lundberg, PhD (Investigation: Supporting; Validation: Supporting; Writing – original draft: Supporting)
 Ilse Rومان, PhD (Methodology: Supporting; Supervision: Supporting; Validation: Supporting)
 Yue J. Wang, PhD (Data curation: Equal; Formal analysis: Equal; Visualization: Equal; Writing – original draft: Equal)
 Meritxell Rovira, PhD (Conceptualization: Lead; Funding acquisition: Lead; Investigation: Lead; Methodology: Supporting; Supervision: Lead; Writing – original draft: Lead)

Conflicts of interest

The authors disclose no conflicts.

Funding

This research was supported by Ministerio de Ciencia, Innovación y Universidades (MICIN) (PID2019-106160RB-I00, PID2022-136973OB-I00, and Cancer Research Innovation in Science [CRIS] Cancer Foundation Excellence Grant) to Meritxell Rovira. Adrián Holguín-Horcajo was supported through a fellowship from MICIN (PRE2020-092678). This study was partially funded by donations collected through the customers of Bonpreu i Esclat thanks to the Charity Rounding Up developed by Worldcoo. The Centres de Recerca de Catalunya (CERCA) Programme/Generalitat de Catalunya provided institutional support. Jennifer M. Bailey-Lundberg was supported by the National Institutes of Health (R01CA277161). This work was supported by the Research Foundation Flanders (FWO) (FWO research project G0A7322N to Ilse Rومان; Odysseus fellowship G0F8916N to Ilse Rومان; and PhD fellowship 1157221N to Katarina Coolens) and the Research Council VUB (OZR-BOF): Senior Research Fellowship OZRSRF44 to Ilse Rومان and SRP65 project to Ilse Rومان.

Data Availability

Data are available at the Gene Expression Omnibus repository with accession number GSE262292.

Supplementary Methods

Chronic Pancreatitis

For the induction of chronic pancreatitis, 8–12-week-old C57BL/6 mice were treated with 125 $\mu\text{g}/\text{kg}$ caerulein. Mice received hourly intraperitoneal injections every other day (6 injections/day at days 0, 2, and 4) for 6 days and then received single daily injections until day 65 in cycles of 5 injection days + 2 injection-free days. Mice were culled at day 65.

Whole Pancreatic Duct Isolation and Purification

Mouse pancreas was dissected from 8–12-week-old mice. Pancreas was minced in phosphate-buffered saline (PBS), and the fragments were transferred to digestion buffer (Hank's balanced salt solution medium containing 1.5–1.7 U/mL collagenase P) and then incubated for 10–15 minutes at 37°C, with the digestion mix vigorously shaken every 3–4 minutes. After digestion, the collagenase-containing buffer was neutralized by adding 10 mL of blocking buffer (5% volume/volume [v/v] fetal bovine serum [FBS] in Hank's balanced salt solution). The tissue digest was centrifuged at 300g at 4°C for 5 minutes. The supernatant was removed, and the pellet was washed twice using 10 mL of blocking buffer. The pellet was resuspended in 10 mL of blocking buffer. The digested pancreas was placed in petri dishes, and whole ducts were hand-picked and sorted by size under a fluorescent stereoscope and transferred into a new tube in ice-cold fresh blocking buffer.

Ductal Cell Single-Cell Prep

Medium and big ducts were further digested with collagenase P (1.5–1.7 U/mL) for 5–10 minutes at 37°C, with the digestion mix vigorously shaken every 2–3 minutes. After digestion, collagenase P was washed twice. Finally, all samples (small, medium, and big ducts) were further digested using 1 mL of tryPLE Express for 5–10 minutes (depending on the size of the ducts) at 37°C, with the digestion mix vigorously shaken every 2–3 minutes. After digestion, tryPLE was neutralized by adding 10 mL of blocking buffer, centrifuged, and washed twice. Purified single ductal cells were resuspended in FACS buffer (10% v/v FBS, PBS). The cell suspension was filtered using a 70- μm and 40- μm cell strainer.

Cell Staining and Fluorescence-Activated Cell Sorting Analysis

Cell suspensions were washed using FACS buffer. Secondary antibody incubation, when primary antibodies were not conjugated to a fluorochrome, was performed on ice for 30 minutes in FACS buffer with secondary antibody (1:300 dilution). Samples were washed twice before FACS analysis or cell sorting. All the incubations were performed at 4°C.

All FACS analyses were performed using a Beckman Coulter Gallios Analyzer, and cell sorting was performed using a Beckman Coulter High-Speed Cell Sorter Moflo-XDP.

Flow-derived data were analyzed using Kaluza 2.1 software (Beckman Coulter, Inc).

Culture of Ductal-Derived Organoids

FACS-sorted ductal cells (GFP⁺) or whole ducts were embedded in a Matrigel medium (25% triplePlus Media: 1% v/v Penicillin-streptomycin, 1 mmol/L HEPES, 1 \times GlutaMAX, Advanced DMEM/F12; and 75% Matrigel) at a density of 1000–5000 cells per 40 μL Matrigel dome. Each Matrigel dome was placed in individual wells of a 24-well plate and transferred into a 37°C incubator for gelification for 10 minutes. Domes were covered with pancreatic organoid expansion medium (1 \times B27 minus vitamin A, 1 mmol/L *N*-acetylcysteine, 50 ng/mL Rspo1, 10 mmol/L nicotinamide, 10 nmol/L gastrin, hEGF 50 ng/mL, hFGF10 100 ng/mL, hNoggin 50 ng/mL, 0.5 $\mu\text{mol}/\text{L}$ A83, 10 $\mu\text{mol}/\text{L}$ prostaglandin E2, triplePlus Media) supplemented with 10 $\mu\text{mol}/\text{L}$ Y-27632 (only for first seeding of single cells). Medium was refreshed every 3–4 days. Organoids were passaged every 5–7 days. For passage, organoids were extracted from the Matrigel using 5–10 mL of ice-cold triplePlus medium, centrifuged at 4°C and 1000 revolutions per minute and washed twice. Pellet was resuspended in 200 μL of triplePlus, and organoids were fragmented by pipetting up and down 22 times using an antiadherent-coated P200 tip. Fragments were washed and resuspended in Matrigel medium and replated in a 1:3–1:6 split ratio.

Endocrine Differentiation Media

Two days after organoid passage, organoids were cultured with differentiation medium 1 (1 \times B27 minus vitamin A, 1 mmol/L *N*-acetylcysteine, 10 mmol/L nicotinamide, 1 \times insulin-transferrin-selenium-ethanolamine, 1 $\mu\text{g}/\text{mL}$ heparin sodium salt, 0.1 $\mu\text{mol}/\text{L}$ γ -secretase inhibitor, 0.1 $\mu\text{mol}/\text{L}$ (amyloid precursor protein 1P, TPB), 50 nmol/L retinoic acid, in triplePlus Media) for 4 days. Upon this first period, the differentiation protocol was followed by using differentiation medium 2 for 4 additional days (1 \times B27 minus vitamin A, 1 mmol/L *N*-acetylcysteine, 10 mmol/L nicotinamide, 1 \times insulin-transferrin-selenium-ethanolamine, 1 $\mu\text{g}/\text{mL}$ heparin sodium salt, 0.1 $\mu\text{mol}/\text{L}$ γ -secretase inhibitor, 0.1 $\mu\text{mol}/\text{L}$ amyloid precursor protein 1P (TPB), 10 $\mu\text{mol}/\text{L}$ Alk5 inhibitor II, in high-glucose triplePlus Media or control medium (1 \times B27 minus vitamin A, 1 mmol/L *N*-acetylcysteine, 10 mmol/L nicotinamide, 1 \times insulin-transferrin-selenium-ethanolamine, 1 $\mu\text{g}/\text{mL}$ heparin, triplePlus Media). Media was refreshed every other day. See [Supplementary Table 2](#) for reagent references.

Pancreas Staining and Microscopy Analysis

Samples were fixed in 4% paraformaldehyde and washed with PBS 3 times. Whole pancreas was fixed at 4°C overnight, and whole ducts and cultured organoids were fixed for 20–30 minutes. If used for paraffin sectioning, samples were immediately taken for automatic paraffin inclusion.

For paraffin-embedded samples, pancreas or organoids were sectioned at 4–5 μm . Antigen retrieval was performed after deparaffinization using citrate buffer pH6 in a decloaking chamber. After 1 hour of blocking with 0.5% v/v triton, 5% v/v FBS, and PBS, tissue sections were incubated with primary antibodies (see [Supplementary Table 2](#))

overnight at 4°C, followed by 3 washes using blocking buffer and incubated with secondary antibodies for 2 hours at room temperature, followed by 3 PBS washes, before 4',6-diamidino-2-phenylindole (DAPI) staining for 15 minutes at room temperature. After 3 additional PBS washes, coverslips were mounted using Fluoromount-G (SouthernBiotech).

For whole-mount staining, fixed whole ducts and cultured organoids were incubated for 1 hour at room temperature with block buffer and then incubated with primary antibodies overnight at 4°C, followed by 3 washes using blocking buffer and centrifugation, incubated with secondary antibodies for 2 hours at room temperature, followed by 3 PBS washes, before DAPI staining for 15 minutes at room temperature. For imaging, organoids and ducts were placed in mounting media (Dako) on a glass bottom microwell dish (MatTek).

All confocal images were captured by a Leica TCS SP5 inverted confocal microscope. Epifluorescent images were acquired on a Zeiss Axio Observer Z1 with an Apotome inverted fluorescent microscope. Brightfield images of cultured organoids were taken on a Leica Z16 APO vertical stereomicroscope. Organoid sizes were measured using ImageJ/FIJI. Quantification of marker expression on organoids was performed using the Imaris 9.6 software.

Sample Preparation Protocol for Frozen Tissue Sections for MACSima

Before immunofluorescence staining, frozen tissue was prepared according to the manufacturer's protocol (Miltenyi Biotec B.C. & Co.KG). In brief, MACSWell Imaging (Miltenyi Biotec) frames were mounted directly on the objective slide. Pretreated (4% PFA over 8 hours, 30% sucrose overnight) frozen sections of 8- μ m tissue thickness were washed 3 times with MACSima Running buffer (no. 130-121-565, Miltenyi Biotec) and subsequently stained with DAPI solution (component of MACSima Stain Support Kit: no. 130-127-575) in the dark for 10 minutes at room temperature. After 3 washing steps with MACSima Running buffer, tissue slices were blocked using 10% v/v bovine serum albumin for 20 minutes at room temperature. Finally, tissue slices were covered with an appropriate volume of MACSima Running buffer to each well depending on the used MACSWell Imaging Frame and samples loaded into the MACSima Imaging System.

MACSima Imaging Cyclic Staining Technology Using the MACSima Imaging System

As a fully automated instrument, the MACSima Imaging System (Miltenyi Biotec) combines liquid handling with widefield microscopy for cyclic immunofluorescence staining. In brief, staining cycles consisted of the following automated steps: immunofluorescent staining, sample washing, multifield imaging, and signal erasure by photo-bleaching. Incubation time was adapted for some markers to 30 minutes, and antibody concentrations were optimized individually. Antibodies used for used for cyclic

immunofluorescence staining with the MACSima Imaging Platform are included in [Supplementary Table 2](#).

Image Analysis Using MACSiQ View Imaging Software

The acquired images by the MACSima (single field of views) were preprocessed using MACSiQ View Imaging Software (analysis module, Miltenyi Biotec) for stitching, registration, and background subtraction according to the current Pre-Processing-Pipeline (Miltenyi Biotec). Preprocessed data were segmented to identify individual ductal cells using DAPI (for cell nuclei) and endogenous GFP (for nuclei and cytoplasm) followed by antibody staining for each marker being analyzed.

Bioinformatic Analysis Comparison With Human Pancreatic Ductal Adenocarcinoma Samples and Mouse Pancreatic Intraepithelial Neoplasia

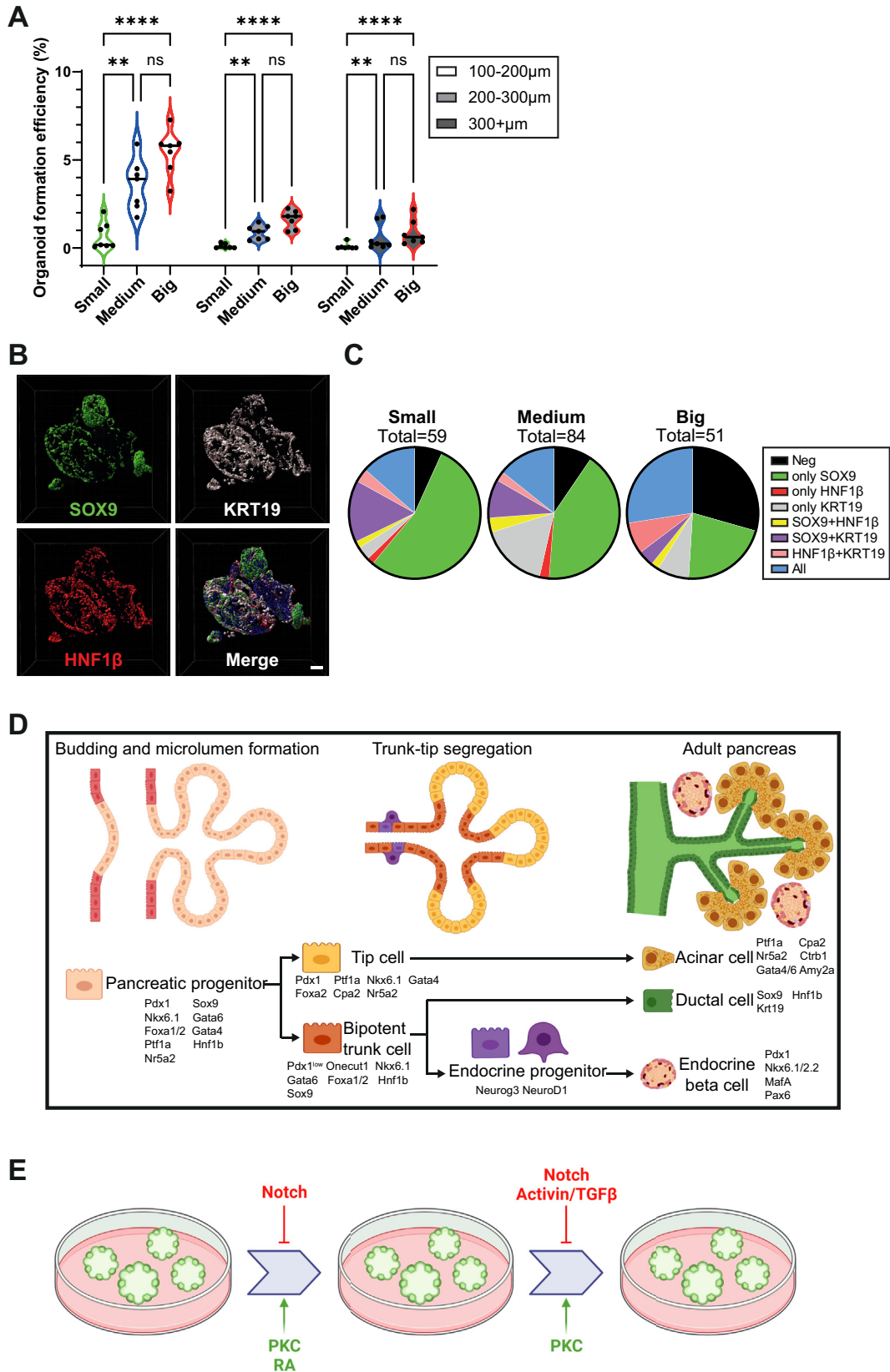
The "AddmoduleScore" function from Seurat was used to assess the resemblance between these ductal cell populations and malignant ductal cells in mouse PanIN and human PDAC. Module scores were computed with default parameters except the adjustment of $\text{ctrl}=20$ for mouse PanIN. Human PDAC was downloaded from GSA: CRA001160,^{e1} and mouse PanIN data were downloaded from GSE141017.^{e2} Cell annotations for human PDAC were provided within the depository. Cell annotation for mouse PanIN was processed based on the criteria outlined in the original study. Specifically, ductal cells were identified as tdTomato^+ , Cpa^- , and Krt19^+ ; metaplastic cells as tdTomato^+ , $\text{Cpa}1^-$, Krt19^+ ; and acinar cells as tdTomato^+ , $\text{Cpa}1^+$, Krt19^- .

Gene Ontology Analysis

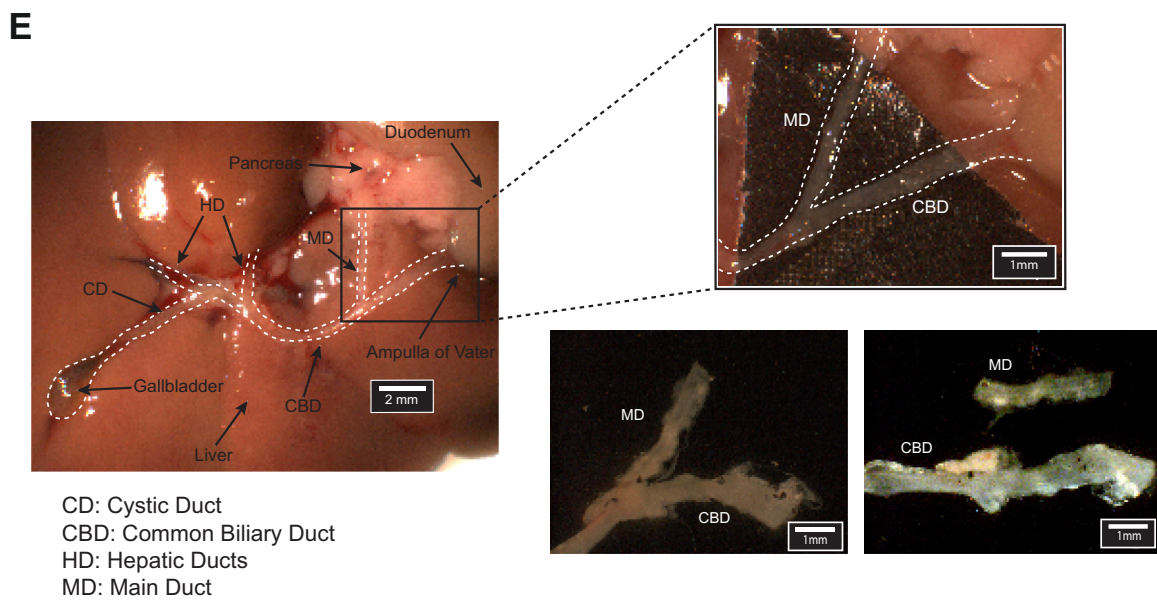
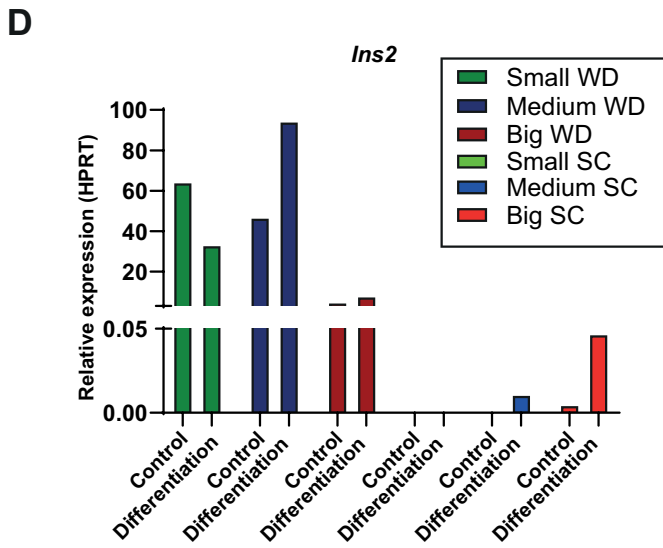
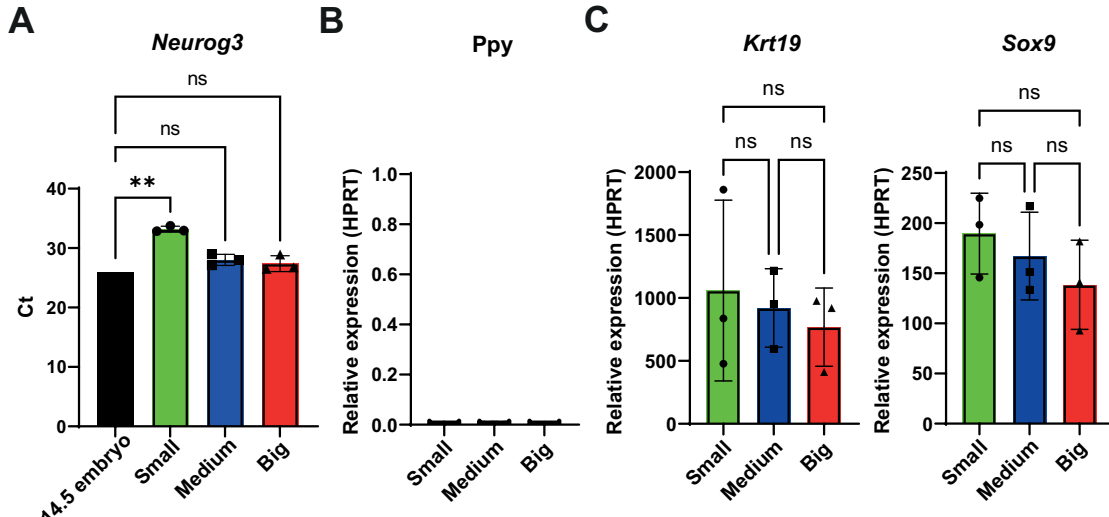
Gene Ontology analysis has been computed with the R package gprofiler2^{e3} (version 0.2.1). The gprofiler2:goset function was run with the genes belonging to each cluster and limiting the background to genes that showed detectable expression in at least 3 cells in the expression matrix.

Supplementary References

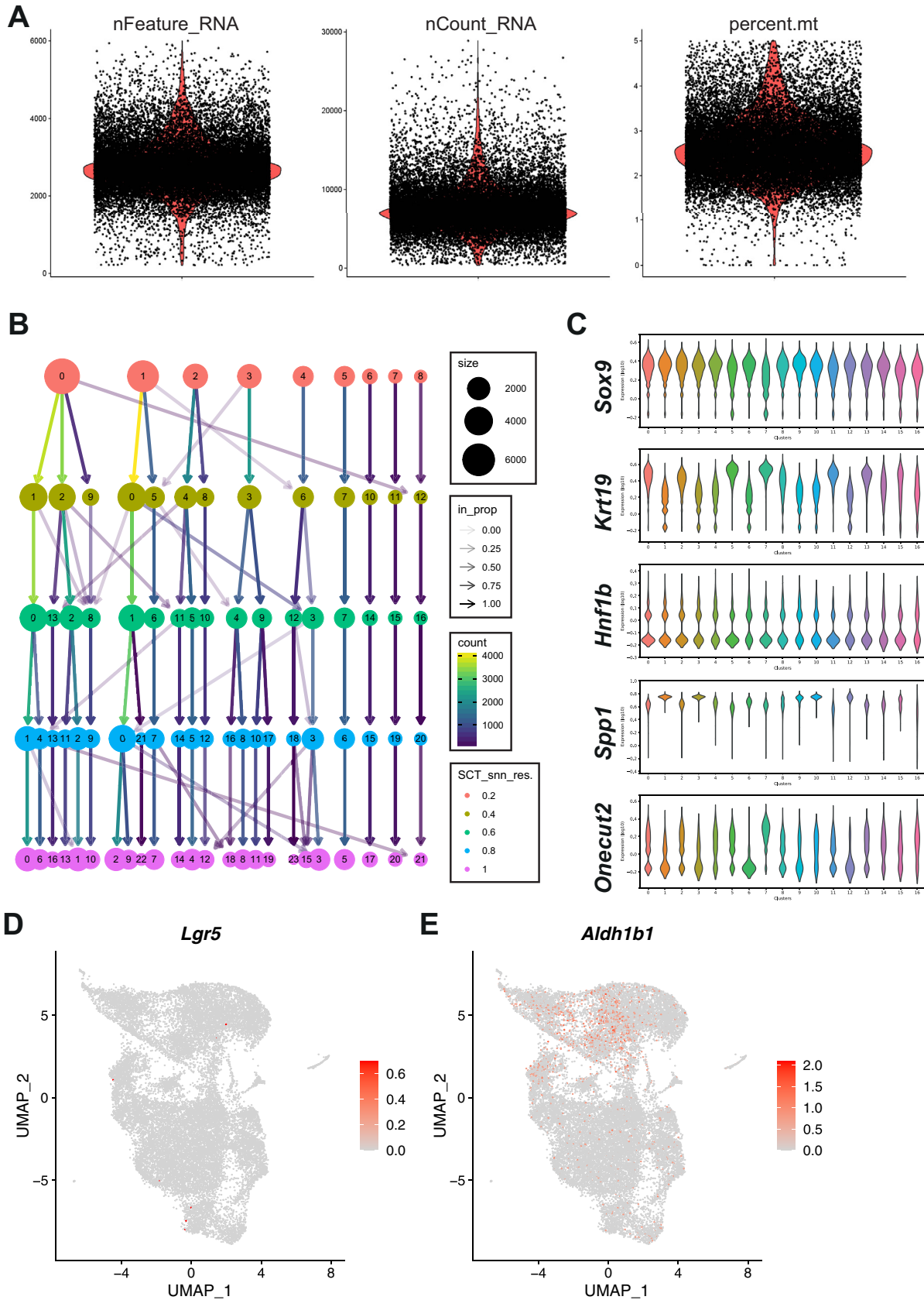
- e1. Peng J, Sun BF, Chen CY, et al. Single-cell RNA-seq highlights intra-tumoral heterogeneity and malignant progression in pancreatic ductal adenocarcinoma. *Cell Res* 2019;29:725–738.
- e2. Schlesinger Y, Yosefov-Levi O, Kolodkin-Gal D, et al. Single-cell transcriptomes of pancreatic preinvasive lesions and cancer reveal acinar metaplastic cells' heterogeneity. *Nat Commun* 2020;11(1):4516.
- e3. Kolberg L, Raudvere U, Kuzmin I, et al. gprofiler2—an R package for gene list functional enrichment analysis and namespace conversion toolset g:Profiler. *F1000Res* 2020;9(ELIXIR):709.
- e4. Malinova A, Veghini L, Real FX, et al. Cell lineage infidelity in PDAC progression and therapy resistance. *Front Cell Dev Biol* 2021;9:795251.



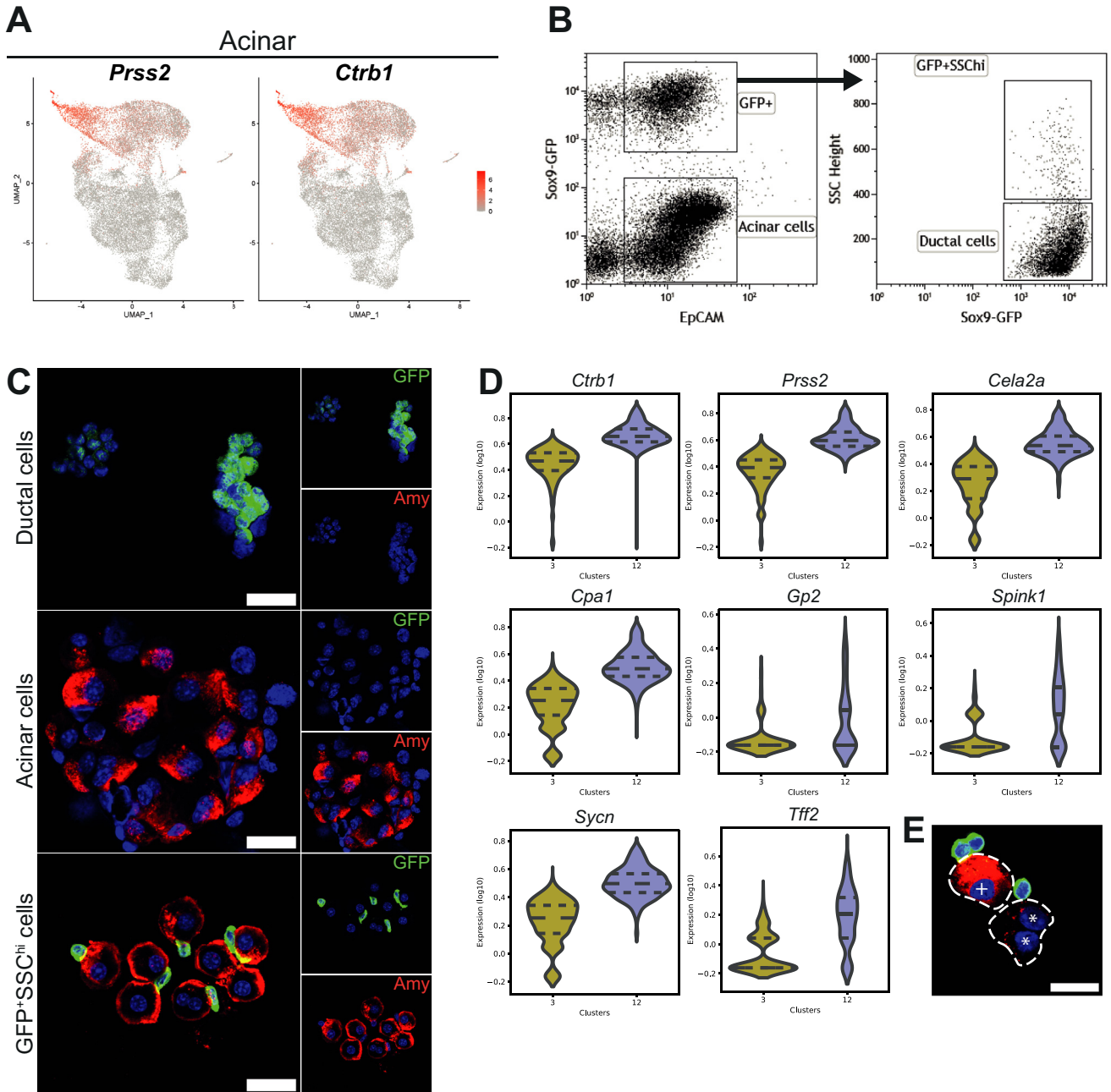
Supplementary Figure 1. Organoid characterization. (A) Violin plot showing organoid formation efficiency and size of small (*green*), medium (*blue*), and big (*red*) ductal-derived organoids generated from isolated single-cell cultures. Size from 100–200 μm , 200–300 μm , and over 300 μm of diameter (1-way analysis of variance, Tukey post hoc test, $n = 7$). (B) Representative whole-mount immunofluorescence images of organoids showing heterogeneous expression of Sox9 (*green*), HNF1 β (*red*), Krt19 (*white*), and nuclei (DAPI, *blue*). Scale bar, 100 μm . (C) Pie charts showing the heterogeneity of expression of the mentioned markers in organoids derived from small, medium, and big ducts. (D) Schematic representation of pancreatic development, showing some of the key genes involved in lineage transitions (created with [BioRender.com](https://www.biorender.com); adapted from Malinova et al⁶⁴ with permission). (E) Schematic representation (created with [BioRender.com](https://www.biorender.com)) of the differentiation protocol used to induce organoid differentiation toward endocrine lineage. Neg, negative; PKC, protein kinase C, RA, retinoic acid; TGF, transforming growth factor.



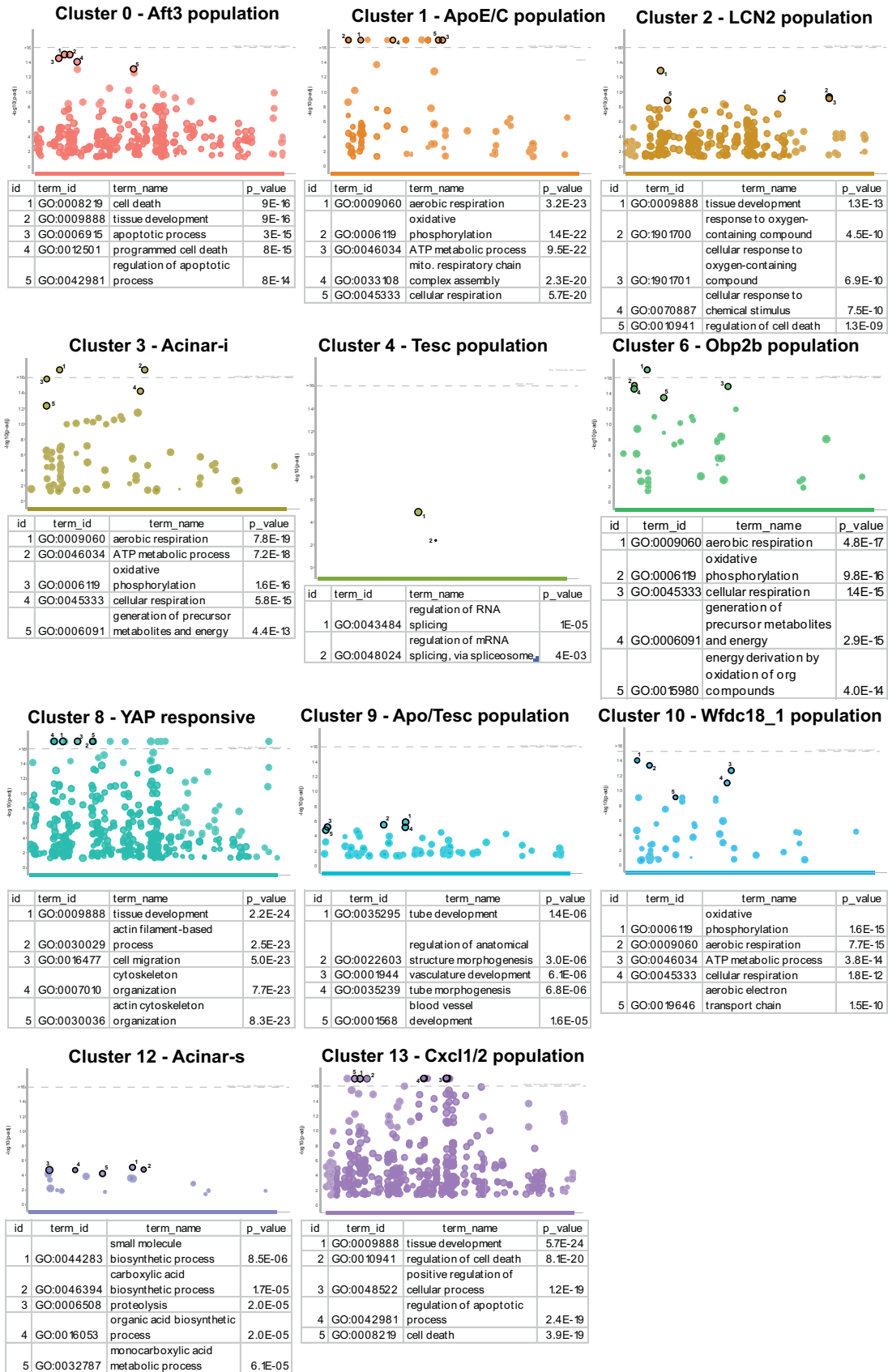
Supplementary Figure 2. Organoids display increased differentiation potential into endocrine progenitors. (A) *Neurog3* mRNA levels in organoids upon differentiation compared to E14.5 embryonic pancreas (1-way analysis of variance, Tukey post hoc test vs embryonic pancreas, N = 3). (B) mRNA expression levels of *Ppy* in differentiated organoids. (C) mRNA expression levels of ductal markers (*Krt19* and *Sox9*) in differentiated organoids (1-way analysis of variance, Tukey post hoc test, N = 3). (D) Insulin mRNA levels in organoids derived from whole ducts (WD) and FACS-isolated single ductal cells from small, medium, and big ducts in differentiation and control media. (E) Brightfield images of common biliary duct and main duct dissection. Pancreas was partially removed to image the common biliary duct and the main duct. Images include gallbladder, cystic duct (CD), hepatic ducts (HD), common biliary duct (CBD, including the pancreatobiliary duct), main duct (MD), ampulla of Vater, and duodenum. HPRT, hypoxanthine phosphoribosyltransferase 1; SC, single cell. Scale bar, 50 μ m.



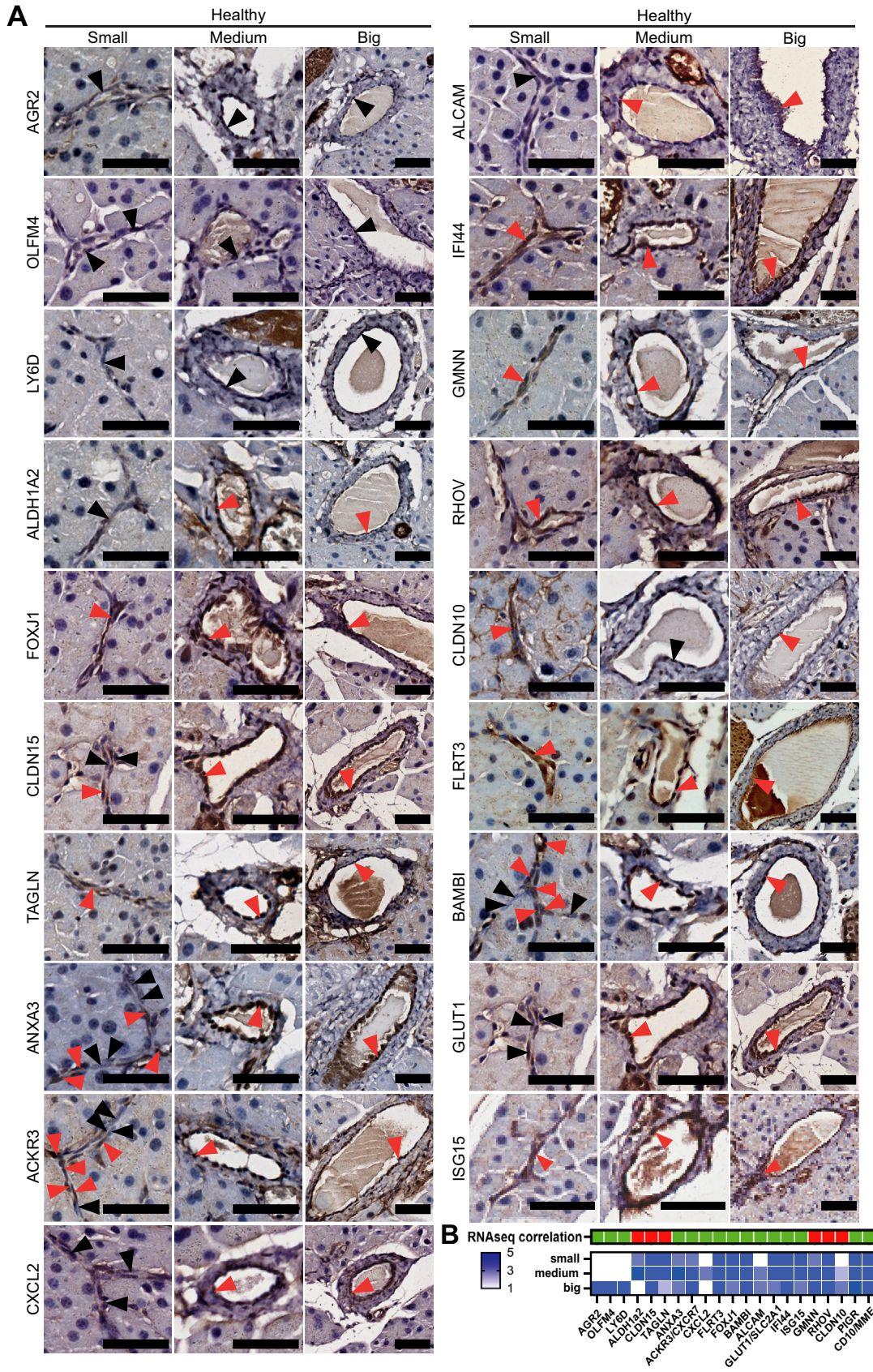
Supplementary Figure 3. Quality control of scRNA-seq samples. (A) Quality control plots indicating nFeature_RNA: number of genes detected per cell; nCount_RNA: number of UMIs per cell; and percent.mt: percentage of mitochondrial genes. (Low-quality/dying cells often exhibit extensive mitochondrial contamination.) (B) Clustering tree. This visualization shows the relationships between clusters at multiple resolutions. (C) Violin plots showing expression of ductal markers in all identified clusters. (D) UMAP plot showing *Lgr5* expression in our scRNA-seq dataset. (E) UMAP plot showing *Aldh1b1* expression in our scRNA-seq dataset.



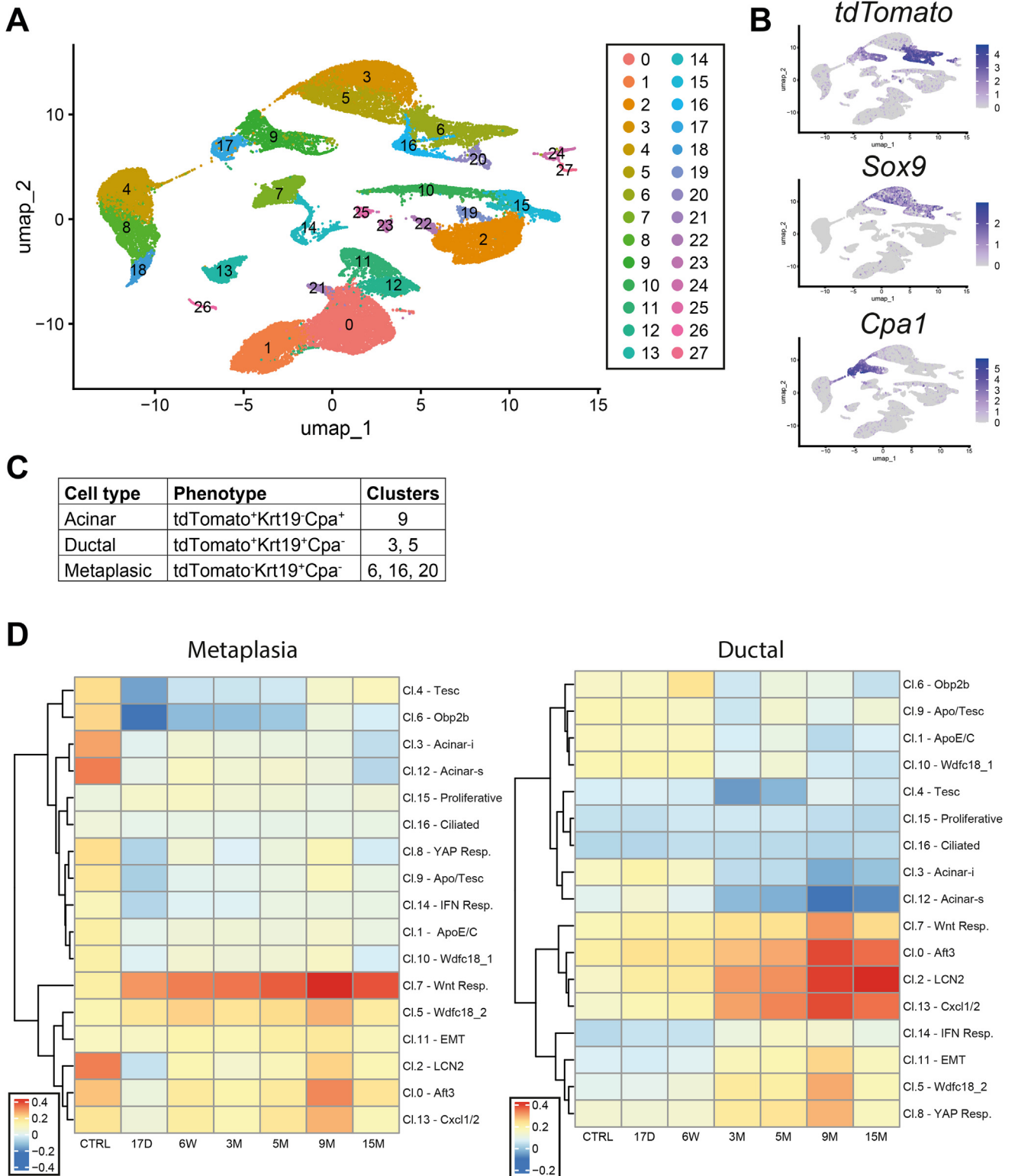
Supplementary Figure 4. Acinar contamination. (A) UMAP plots showing the expression of acinar cell markers (*Prss2* and *Ctrb1*). (B) Representative flow cytometry plots showing the FACS sorting strategy to isolate acinar cells (EpCAM⁺Sox9:eGFP⁻), ductal cells (EpCAM⁺Sox9:eGFP⁺SSC^{low}), and acinar cells expressing GFP (EpCAM⁺Sox9:eGFP⁺SSC^{high}). (C) Immunofluorescence staining on cytopun freshly isolated ductal, acinar, and acinar/eGFP-positive sorted cells for GFP (green, readout for Sox9 expression) and amylase (red, acinar marker). Scale bar, 50 μ m. (D) Violin plots showing the expression of acinar genes *Ctrb1*, *Prss2*, *Cela2a*, *Cpa1*, *Gp2*, *Spink1*, *Syncn*, and *Tff2* on clusters 3 and 12. (E) Immunocytochemistry staining on cytopun freshly isolated acinar sorted cells. Dashed lines highlight the acinar cells, * indicates an acinar binucleated cell with low levels of amylase (red), and + indicates a mononucleated acinar cell with high levels of amylase. Scale bar, 50 μ m.



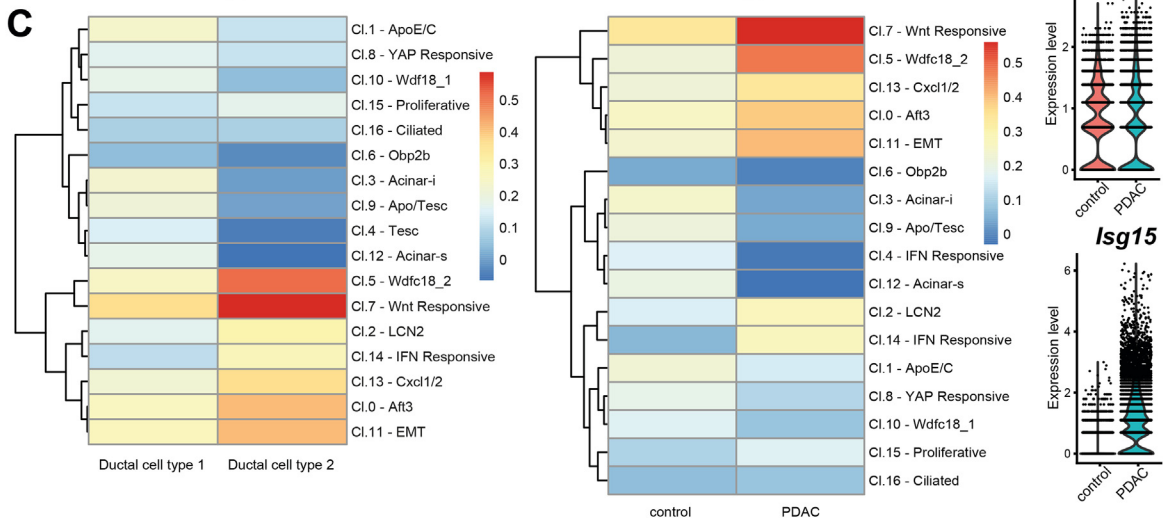
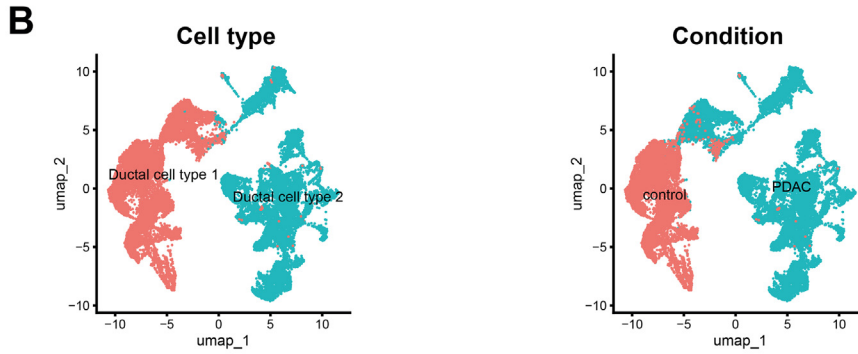
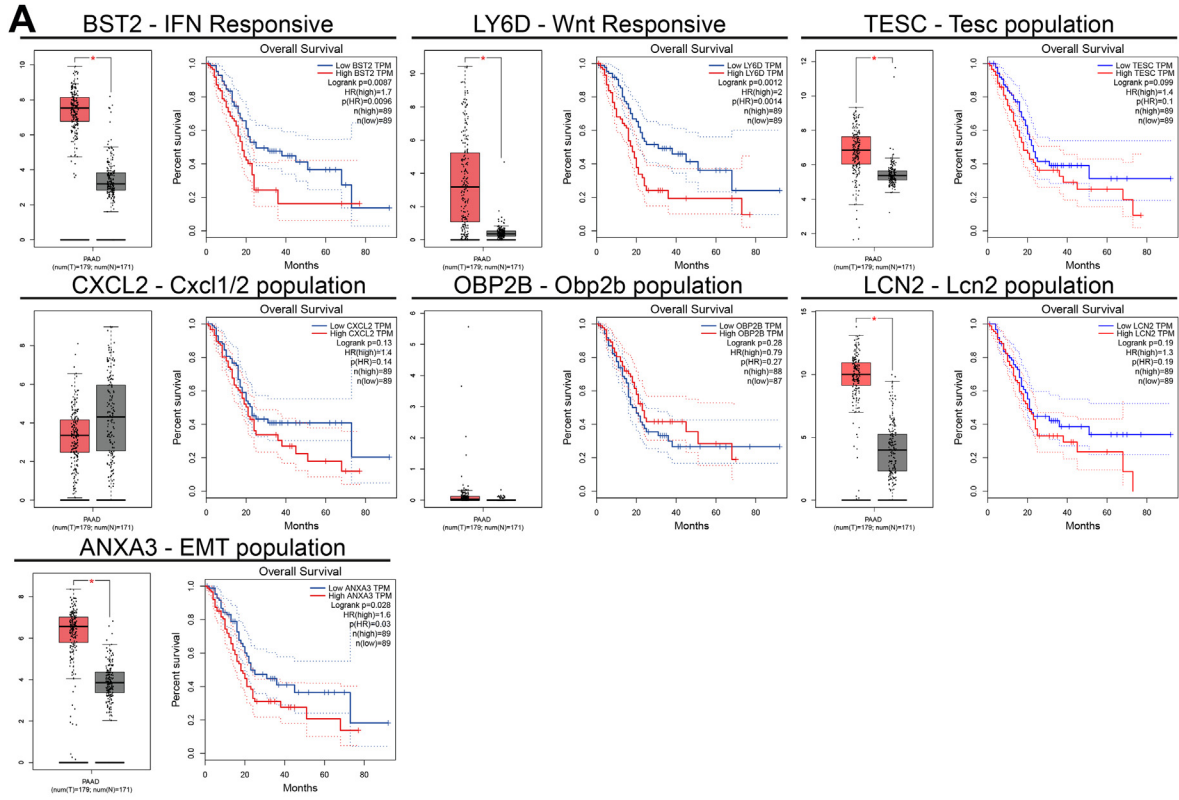
Supplementary Figure 5. Gene Ontology. Plots showing Gene Ontology analysis for ductal clusters 0–4, 6, 8–10, 12, and 13, with the top 5 significant Gene Ontology terms. GO, Gene Ontology.



Supplementary Figure 6. Detection of novel ductal markers in healthy pancreatic tissue. (A) Representative images of immunohistochemistry detection of *Cldn15*, *Tagln*, and *Anxa3* (EMT population); *Ackr3* (YAP-responsive population); *Cxcl12* (Cxcl1/2 population); *Flrt3* (medium-big ducts); *Bambi* (ciliated population); *Glut1* (expression in some ductal cells); *Isg15* (IFN-responsive population) in healthy pancreas; *Agr2*, *Olfm4*, and *Ly6D* (Wnt-responsive population); *Aldh1A2* (medium-big clusters); *FoxJ1* (ciliated population); *Alcam* (panductal); *Ifi44* (IFN-responsive population); *Gmnn* (enriched in small-derived clusters); *RhoV* (enriched in small-derived clusters); and *Cldn10* (enriched in small-derived clusters) in healthy small, medium, and big ducts (*red arrows* indicate positive cells, and *black arrows* negative cells). *Scale bar*, 50 μm . (B) Heatmap plot shows qualitative correlation (*green*) or no correlation (*red*) between protein expression and scRNA-seq data. Heatmap plot shows, in *blue*, qualitative analysis of marker expression in small, medium, and big ducts in healthy tissue.



Supplementary Figure 7. Mouse PDAC comparison. (A) UMAP plots of pancreatic populations identified by Schlesinger et al^{e2} in PDAC mouse samples. (B) UMAP plots showing tdTomato expression (indicating Tomato positive cells traced from the mouse line used in the study^{e2}), Sox9 expression (ductal marker) and Cpa1 expression (acinar marker). (C) Table summarizing acinar, ductal and metaplastic clusters identified. (D) Heatmap plots showing the transcriptional profile comparison between our scRNAseq data and Schlesinger et al^{e2} showing that the transcriptional signatures of big duct-derived populations, including the Wnt-responsive and EMT populations (and to a lesser extent IFN-responsive) were higher expressed in ductal and metaplastic cells in tumor samples.



Supplementary Figure 8. Human PDAC comparison. (A) mRNA expression of population markers *BST2* (IFN-responsive population), *LY6D* (Wnt-responsive population), *TESC* (Tesc population), *CXCL2* (Cxcl1/2 population), *OBP2B* (Obp2b population), *LCN2* (Lcn2 population), and *ANXA3* (EMT population) in human PDAC samples and healthy pancreas via GEPIA (<http://gepia.cancer-pku.cn/>) database including TCGA and genotype-tissue expression (GTEx) data. Box plot represents tumor (T) in red (179 samples) and normal tissue (N) in gray (171 samples). X-axis represents mRNA expression as $\log_2(\text{TPM}+1)$. Significant differences are shown ($^*\alpha < 0.001$). Kaplan-Meier survival curves are plotted using GEPIA where median group survival cutoff of 50% is shown, as well as hazard ratios and 95% confidence intervals. (B) UMAP plots of ductal populations in human samples (normal and PDAC) from Peng et al.^{e1} (C) Heatmap plots showing transcriptional profile comparison between our scRNAseq data and Peng et al.^{e1} ductal cell types 1 and 2 (being ductal cell type 2 the “malignant” subtype) and heatmap showing transcriptional profile comparison between control (normal pancreas) and PDAC samples from the same study). (D) Violin plots showing expression of population specific markers from Wnt-responsive population (*AGR2*), IFN population (*ISG15*), and EMT population (*ANXA3*) in control and PDAC samples from Peng et al.^{e1}

